POLITECNICO DI MILANO

Scuola di Ingegneria Industriale e dell'Informazione

Corso di Laurea Magistrale in Ingegneria Biomedica

POLITECNICO
MILANO 1863

Setting up of a neuroblastoma cell invasion dynamic 3D model inside a millifluidic optically accessible bioreactor

Relatore: Prof.ssa Emanuela Jacchetti

Correlatori: Ing. Simone Perottoni

Prof.ssa Manuela Teresa Raimondi

Dott. Sanja Aveic

Tesi di laurea di: Francesco Minozzi

Matricola: 905077

Anno Accademico 2020/2021

Index

Abstract 1
Sommario 3
1. Introduction 4
1.1 Neuroblastoma 4
1.1.2 Pathology and clinical presentation 4
1.1.3 Staging and risk classification 5
1.1.4 Embryonic origin 7
1.1.5 EMT and peripheral sympathetic nervous system formation 8
1.1.6 Neuroblastoma Biology 10
1.1.7 MYCN amplification 11
1.1.8 ALK mutations 11
1.1.9 Overexpression of LIN28B 12
1.2 Neuroblastoma Models 13
1.2.1 Multicellular Tumour Spheroids (MCTSs) and Bio-printing 15
1.2.2 Scaffold-based platforms and hydrogels 17
1.2.3 Bioreactors and MOAB 18
1.3 Aim of the study 21
2. Materials and methods 22
2.1 SH-SY5Y cell culture 22
2.2 Fluorescent Cell Labelling 23
2.3 MOAB 25
2.3.1 Modelling for dynamic culture 27
2.3.2 MOAB set up protocol 29
2.4 LIVE/DEAD assay 32
2.5 Time-Lapse 32
3. Results 33
3.1 MOAB set up 33
3.1.1 Flow rate 33
3.1.2 Number of cells and amount of growth medium 35
3.1.3 Dye selection 41
3.2 LIVE/DEAD assay 44
3.3 Time lapse and cells migration 46
4. Discussion 50
5. Bibliography 54

Abstract

Neuroblastoma is a pediatric tumor that originates from neural crest cells (NCCs), characterized by a high heterogeneity that affects the clinical conditions of patients. LIN28B, an important gene in embryonic development, has a key role in the formation and progression of several diseases when not physiologically expressed. Indeed, an overexpression of LIN28B leads to an impaired differentiation of sympathoadrenal precursors leading to neuroblastoma genesis in addition to enhancing the cell migration and invasion. Among the new bioengineered devices that could overcome the limitations of the gold standard 2D culture for neuroblastoma tumor cells, we count the miniaturized optically accessible bioreactor (MOAB), able to replicate *in vitro* both 2D and 3D cultures provided with a constant flow of growth medium. In this study we investigated a suitable protocol for human neuroblastoma cancer cell line SH-SY5Y in MOAB, in 2D and 3D in nichoid to confirm in real-time the migratory and invasive phenotypes of SH-SY5Y^{LIN28B} overexpressing LIN28B.

This work was supported by the Neuroblastoma laboratory, Fondazione Istituto di Ricerca Pediatrica Città della Speranza (Padua, Italy), supervised by Dott. Aveic Sanja and assisted by the neuroblastoma team (Dr. Corallo Diana and Miss Pantile Marcella). We focused on determine the most suitable number of cells to be plated, flow rate (respective shear stress) and amount of growth medium to be provided to cells, choice of dye for fluorescent live-cell analysis. Finally, after assessing the viability of cell cultures by LIVE/DEAD assay, we performed a Time Lapse imaging for migratory analysis.

The results obtained in dynamic conditions statistically confirmed an increase of cell motility of neuroblastoma cells due to overexpression of LIN28B, both in terms of distance and speed. There was no significant difference between SH-SY5Y^{LIN28B} cells cultured in 2D and 3D in nichoid, even though different patterns of migration were observed. Hence, further investigations will lead in future to a better understanding of 3D structures in dynamic conditions, permitting to exploit all its potentiality as disease model.

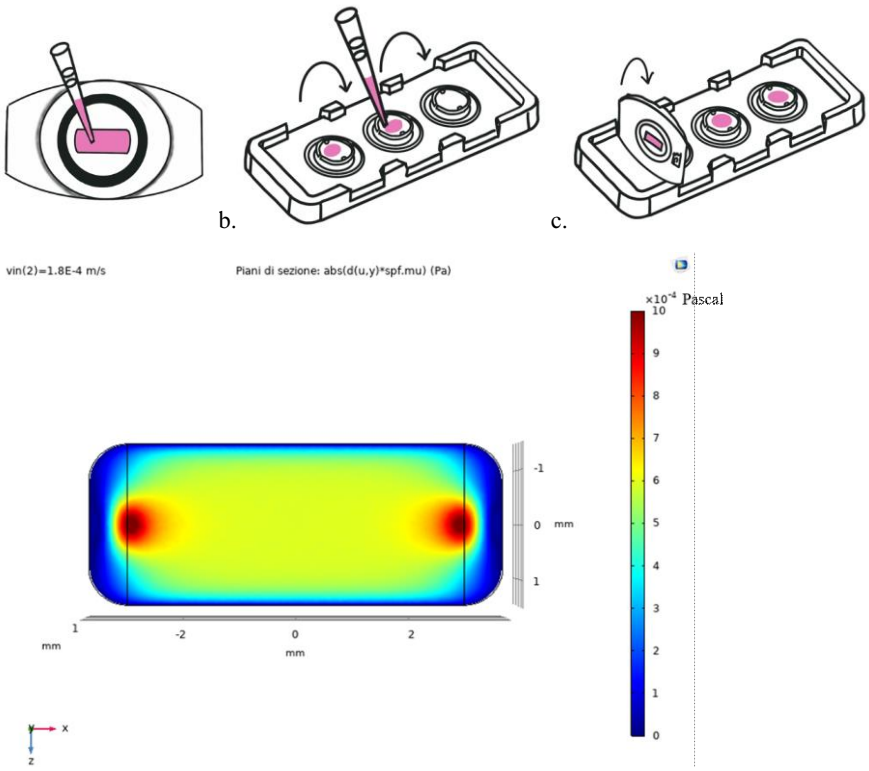

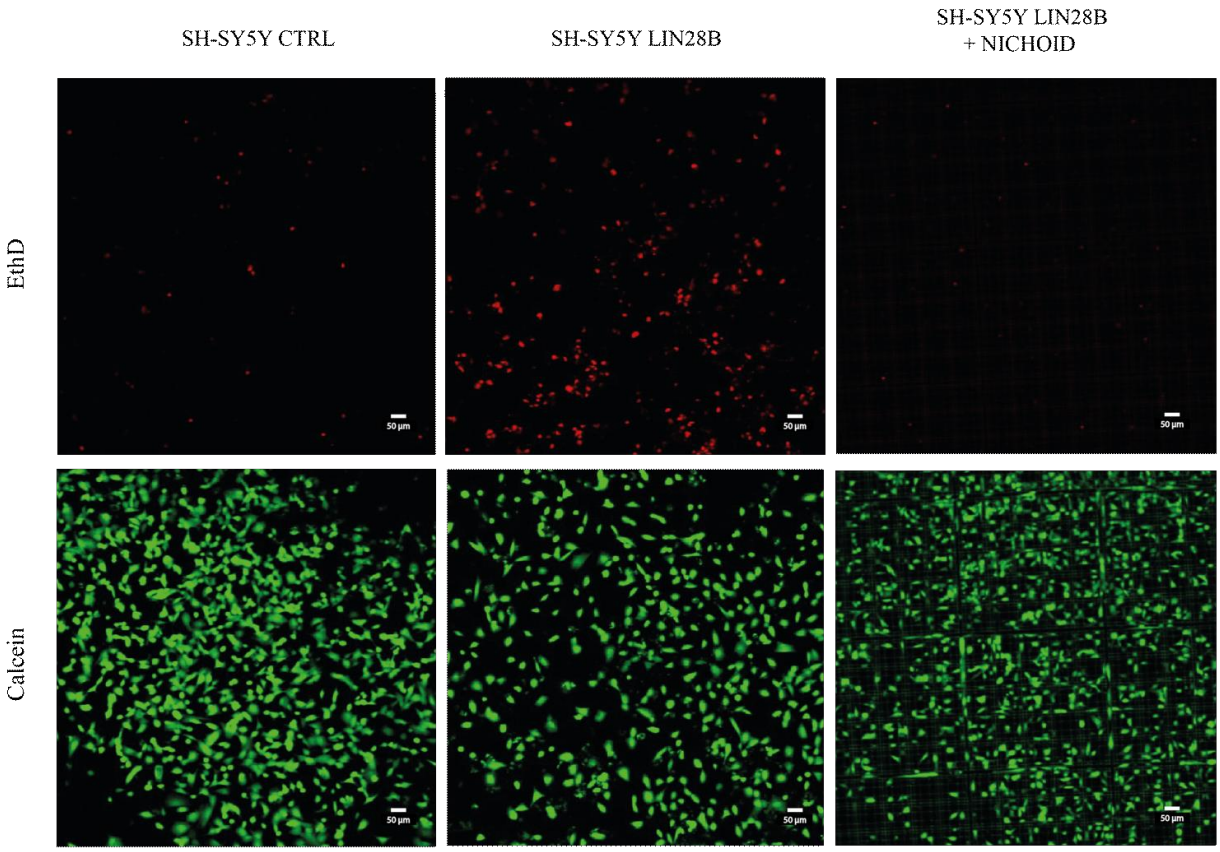

(Up) *Technical sketches of miniaturized optically accessible bioreactor (MOAB)****. (Middle)*** *COMSOL Multiphysics® simulation of shear stress inside the MOAB chamber with set 5.0 × 10^{-3} mL/min flow rate.* ***(Low)*** *LIVE/DEAD assay for SH-SY5Y^{CTRL} and SH-SY5Y^{LIN28B} in absence or presence of nichoid inside MOAB chambers.*

Sommario

Il neuroblastoma è una forma tumorale pediatrica che origina da cellule della cresta neurale (NCCs), caratterizzato da un'elevata eterogeneità che influenza le condizioni cliniche dei pazienti.
LIN28B, un gene importante per lo sviluppo embrionale, ha un ruolo chiave nella formazione e progressione di diverse tipologie tumorali quando non espresso fisiologicamente. Infatti, una overespressione di LIN28B blocca il differenziamento dei precursori simpatoadrenergici promuovendo in questo modo la formazione di neuroblastoma, oltre a favorire la migrazione e invasività cellulare.
Tra i nuovi dispositivi di bioingegneria che potrebbero superare i limiti delle colture cellulari in 2D, il gold standard per lo studio in oncologia di neuroblastoma, si può annoverare il miniaturized optically accessible bioreactor (MOAB), un bioreattore capace di replicare *in vitro* entrambe le colture 2D e 3D mantenendo una condizione dinamica con un costante flusso di medium di crescita alle cellule. In questo studio abbiamo indagato le migliori condizioni per poter effettuare una coltura 2D e 3D in nichoid di linee cellulari umane di neuroblastoma SH-SY5Y all'interno del MOAB per confermare in tempo reale il fenotipo migratorio e invasivo delle cellule SH-SY5Y^{LIN28B} overesprimenti LIN28B in confronto alle cellule SH-SY5Y^{CTRL} di controllo. Questo lavoro è stato supportato dal laboratorio di Neuroblastoma, Fondazione Istituto di Ricerca Pediatrica Città della Speranza (Padova, Italia), supervisionato dalla Dott. Aveic Sanja e assistito dal team di Neuroblastoma (Dr. Corallo Diana e Sig.ra Pantile Marcella). Ci siamo concentrati sul determinare il numero di cellule più idoneo da seminare, un flusso (e rispettivi shear stress) adeguato a fornire il giusto quantitativo di medium di crescita alle cellule, un colorante ideale per l'analisi live-cell in fluorescenza. Infine, dopo aver confermato la sopravvivenza cellulare in coltura con un'analisi LIVE/DEAD, abbiamo acquisito delle immagini in Time Lapse per lo studio della migrazione cellulare. I risultati ottenuti in condizione dinamica hanno confermato un aumento significativo della motilità cellulare di neuroblastoma dovuta a una overespressione di LIN28B, sia in termini di distanza che di velocità. Non sono state riscontrate invece delle differenze significative tra i dati raccolti dalle culture dinamiche 2D e 3D in nichoid, nonostante siano stati evidenziati dei pattern di migrazioni diversi. Si sottolinea quindi la necessità in futuro di effettuare ulteriori valutazioni per poter comprendere e sfruttare al massimo le potenzialità della coltura tridimensionale in una condizione dinamica, fornendo così un modello tumorale per lo studio di neuroblastoma.

1. Introduction

1.1 Neuroblastoma

Neuroblastoma (NB) is a solid form of cancer developing in extracranial sympathetic nervous system. It is classified as an embryonal tumour, originating from trunk neural crest cells (NCC) that can transform into neuroblasts due to several genetic and epigenetic alterations. This leads to the onset of primary tumours in one or more places all along the sympathetic chain, from the neck to the pelvis, within adrenal gland and paravertebral sympathetic ganglia (Delloye-Bourgeois et al, 2019).

1.1.2 Pathology and clinical presentation

Neuroblastoma is reported as 6-10% of all reported cancer cases in children under 5 years old with an incidence of about 95% within this age, affecting 1 in 8000 live births (Johnsen et al, 2019).
The arise of this malignancy is unusual in adolescents and adults but can be detected. In 2013 in Europe, almost 500 new cases of neuroblastoma were diagnosed (Luksch et al, 2016), with a trend similar to that estimated in the USA with 650 per year (Mahapatra et al, 2020) with more frequency in boys than girls. The link between prenatal development of malignancy and exposure to risk factors during pregnancy is well established in the literature. The most significant is represented by the consumption of alcohol during pregnancy, which leads to an abnormal foetal neuronal development that increases the chance of neuroblastoma onset (Luksch et al, 2016). Other studies highlight a causal association with consumption of tobacco, an occupation with exposure to pesticide or electromagnetic field and the use of oral contraceptives or fertility hormones (Luksch et al, 2016). On the other hand, an oncological investigation exhibits that the inclusion of a dose of folic acid during pregnancy reduces significantly the incidence of neuroblastoma and neural tube defections (French et al, 2003).
About 40% of patients are diagnosed with neuroblastoma at 18 months, and about 90% at less than 10 years of age. The age of diagnosis is strongly correlated to prognosis, indeed patients with less than 18 months of age have much more potential of surviving than others (Matthay et al, 2016).
The location of primary tumours and metastasis takes a critical role in clinical signs and relevant symptoms for neuroblastoma diagnosis. Primary tumours can occur anywhere in the sympathetic nervous system, more than 50% of cases in the medulla of the adrenal glands, this is the clinical condition associated with the most severe cases and lower survival than other sites of primary tumour. The occurrence of tumour in the abdomen involves various symptoms from hypertension, pain and

abdominal distension. Primary tumours that grew in the neck or upper chest often develop Horner's syndrome including ptosis (upper eyelid drop), miosis (pupil constriction) and anhidrosis (lack of sweat) (Kieuhoa et al, 2014 & Lacayo et al, 2017). Tumours developing along the paraspinal sympathetic chain can expand to the spinal column leading to spinal cord compression and in the worst cases resulting in paralysis (Matthay et al, 2016). The chance of neuroblastoma to form metastasis is around 50% of patients, often involving regional lymph nodes, bone marrow and bone, and liver. Metastasis usually lead to symptoms such as bone pain, fever or weight loss. More specifically, bone metastases lead to pain in the diseased bone and to incorrect walking and in rare cases even pathological fracture is reached (Chu et al, 2011); metastases reaching the liver lead to coagulation problems and kidney failure. Metastases to other sites in the body, for instance in lungs or central nervous system, are much rarer events.

1.1.3 Staging and risk classification

A key role to determine the right treatment for patients affected by neuroblastoma is the definition of stages. The most accepted system for their classification is the International neuroblastoma Staging System (INSS), which is based on the local extension of primary tumour and/or metastases revealed at the time of diagnosis. This system divides neuroblastoma tumours into stage 1, 2A, 2B, 3, 4 and 4S (Matthay et al, 2016), (which has 50% of cases of spontaneously regress) that are resumed in Table 1.

1	Localized tumor with complete gross excision, with or without microscopic residual disease; representative ipsilateral lymph nodes negative for tumor microscopically (node attached to and removed with the primary tumor may be positive)
2A	Localized tumor with incomplete gross excision; representative ipsilateral nonadherent lymph nodes negative for tumor microscopy
2B	Localized tumor with or without complete gross excision, with ipsilateral nonadherent lymph nodes positive for tumor. Enlarged contralateral lymph nodes must be negative microscopically
3	Unresectable unilateral tumor infiltrating across the midline*, with or without regional lymph node involvement; or localized unilateral tumor with contralateral regional lymph node involvement; or midline tumor with bilateral extension by infiltration (unresectable) or by lymph node involvement
4	Any primary tumor with dissemination to distant lymph node, bone, bone marrow, liver, skin and/or other organs (except as defined for stages 4S)
4S	Localized primary tumor (as defined for stages 1, 2A or 2B) with dissemination limited to skin, liver and/or bone marrow (limited to infant < 1 year of age)

***** the midline is define as the vertebral column. Tumor originated on one side and crossing the midline must infiltrate to or beyond the opposite side of vertebral column.

Tab. 1: International Neuroblastoma Staging System (INSS) adapted from Brodeur et al, 1993.

Concurrently, other systems were introduced to define different stages of neuroblastoma.
The International Neuroblastoma Risk Group (INRG) Staging System groups together patient considering their conditions before any kind of treatment. Patients are divided into groups according to the location of the disease (L1 and L2) and whether or not it involves vital organs like kidney, liver or

epidural space of the spinal canal; the location of metastasis as distant from the primary tumour (M) or present in liver, skin and bone marrow -only for <18 months age patient- (MS); the genomic characterization focused on the presence or absence of MYCN amplification and ploidy; the histological category and its grade of differentiation (Matthay et al, 2016).

INRG Stage	Age (months)	Histologic Category	Grade of Tumor Differentiation	*MYCN*	11q Aberration	Ploidy	Pretreatment Risk Group
L1/L2		GN maturing; GNB intermixed					A Very low
L1		Any, except GN maturing or GNB intermixed		NA			B Very low
				Amp			K High
L2	< 18	Any, except GN maturing or GNB intermixed		NA	No		D Low
					Yes		G Intermediate
	≥ 18	GNB nodular; neuroblastoma	Differentiating	NA	No		E Low
					Yes		H Intermediate
			Poorly differentiated or undifferentiated	NA			
				Amp			N High
M	< 18			NA		Hyperdiploid	F Low
	< 12			NA		Diploid	I Intermediate
	12 to < 18			NA		Diploid	J Intermediate
	< 18			Amp			O High
	≥ 18						P High
MS	< 18			NA	No		C Very low
					Yes		Q High
				Amp			R High

Tab. 2: International Neuroblastoma Risk Group (INRG) Staging System; Cohn et al, 2009

Hence, this system allows the division of patients into very-low-risk, low-risk, intermediate-risk or high-risk group which leads to proper therapy (Tab 2). The former two includes nearly the 50% of all newly diagnosed neuroblastoma and show an excellent survival, also with cases of complete spontaneous regress. Instead, the latest one has the majority of patients >18 months old and carry the MYCN amplification and other genetic alterations, that lead to worst outcome (Matthay et al, 2016).

1.1.4 Embryonic origin

Neuroblastoma originates from the NCC population (Matthay et al, 2016).

During the development, the neural crest comes up after the closure of the neural tube leading to the delamination of NCC that undergoes an epithelial-to-mesenchymal transition (EMT), migrating and differentiating into a wide range of cell types (Gilbert & Barresi, 2016).

The crest can be divided into four anatomical regions:

- Cranial: cells develop in the mesenchyme of the cranium, differentiating in cartilage, bone, but also cranial neuron, glia, pigment cells and finally face connective tissue;
- Cardiac: subregion of cranial neural crest, which cells specialisation is critical in developing the division between aortas and pulmonary arteries;
- Trunk: migration and differentiation of these cells lead to sympathetic neurons and pigment cells (melanocytes) forming as well as to the medulla section of the adrenal gland;
- Vagal and sacral: fundamental for the development of peristaltic movement in the bowels, as the cells of this region generate the parasympathetic (enteric) ganglia of the intestine.

Both cranial and trunk cells (and the other two regions that overlap with the trunk) are multipotent even though not equivalent, as the cranial NCC can form cartilage, muscle and bone in a specific and unique way.

1.1.5 EMT and peripheral sympathetic nervous system formation

In the developmental stages, NCC undergoes transitional phases, from an epithelial to a mesenchymal phenotype (epithelial-to-mesenchymal transition, EMT) in order to migrate from the neural tube and to differentiate into specific cells (Fig. 1).

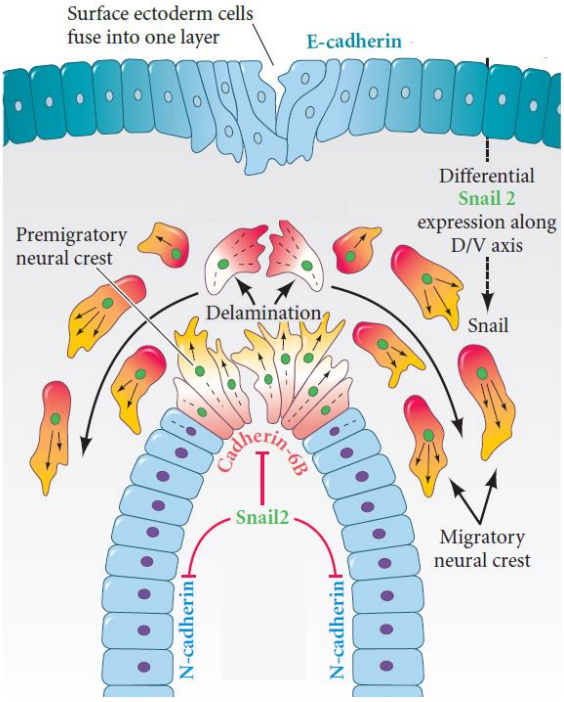

Fig. 1: Neural crest delamination, Gilbert & Barresi, Developmental Biology, 11th ed, 2016

This process is known as delamination and lead to the loss of adhesive cell junctions and in their separation from the epithelium. It has been shown that a number of transcription factors (Sox9, Foxd3 and Snail2) are involved in the initiation of EMT (Raghu et al, 2009).
Crest cells cannot begin migration from the neural tube as long as they remain strongly connected to each other. Adherent junctions are structures formed by membrane proteins that form cell-cell bonds through intracellular junctions called cadherins, which are linked to the cytoskeleton of the cell by actin filaments (connections are also formed with the ECM, through focal adhesions, but instead of cadherins, integrins are involved). In addition to cadherins, claudins and occludins are often involved in tight junctions, playing an important role in cell-cell bond. Thus, during the separation of the neural tube from the ectoderm and the onset of delamination, three separate regions with their own adhesion proteins are formed: E-cadherins for the ectoderm, N-cadherins for the neural tube and cadherins-6b for the promigratory neural crest (Kerosuo et al, 2012). In the complex gene regulation, it is noted how snail repress N-, E- and 6B- cadherins weakening the adherent junction and downregulating the expression of claudine and occludine, this way disrupting as well tight junctions and leading to the migrating pathway (Delloye-Bourgeois et al, 2019). Moreover, an important factor that allows migration is the maintenance of cadrein-6B in the apical zone of promigratory crest cells, which permits the activation of RhoA promoting the formation of actomyosin contractile fibres for apical shrinkage and initiation of delamination and migration (Gilbert & Barresi, 2016).
The fate of trunk NCCs is directly connected to the migratory pathway that they follow.
There are three major pathways after delamination that reflect the waves of migration.
The first one is the ventromedial pathway where NNCs migrate between the neural tube and the developing somite, leading cells to differentiate mainly in sympatho-adrenal cells like neurons and glia of symphatetic glia of ganglia and adrenal medulla cromaffin cells.
The second one is the ventrolateral pathway, in which cells are directed to the rostal part of the somite, developing in dorsal root ganglia neurons and ventral Schwann cells, only few of them choose a sympathetic fate. Is also relevant that trunk NNC which choose a ventral pathway, stop their migration when close to the DA endothelium; the trunk NCCs adjacent to the aortic wall participate to the hemogenic activity and to the differentiation of HSCS that mostly reside in the bone marrow (Delloye-Bourgeois et al, 2019). Lastly, the third wave follows the dorsolateral pathway between the somite and the ectoderm, contributing mostly to the generation of pigment cells of epidermis (Delloye-Bourgeois et al, 2019).

1.1.6 Neuroblastoma Biology

During normal sympatho-adrenal cell differentiation, NNCs express a variety of genes, including the proto-oncogene *MYCN*, *ALK* and *LIN28B*. Their expression is regulated over time with increasing degradation as the cells differentiate into sympathetic neurons. A series of gene alterations leads to the loss of this fine gene regulation, resulting in amplification of *MYCN*, mutations in ALK and overexpression of *LIN28B*; prolonged expression of these genes, by sympatho-adrenal precursor cells, leads to the genesis of neuroblastoma. These data have been supported by research following several *in vivo* studies on transgenic animal models, for example shown in Corallo et al 2016 and 2019 studies.
Neuroblastoma is identified by small blue round cells neoplasm in childhood; indeed, neuroblastoma cells show small shapes with abundant nucleus and few cytoplasms, with some neuritis all over the cell body (Tonini et al, 2016). Neuroblastoma is part of Neuroblastic Tumors, which comprised a group of neoplasm highly heterogeneous in terms of biological, genetic and morphological characteristics.
Neuroblastic Tumors are classified based on the presence of stromal schwannian cell in four categories: neuroblastoma (Schwannian stroma-poor), Ganglio neuroblastoma intermixed (Schwannian stroma-rich), Ganglioneuroma (Schwannian stroma-dominant) and Ganglioneuroblastoma nodular (mix of Schwannian stroma-rich, dominant and poor) neuroblastoma, and by definition of this category, has the rate of tumour tissue with stroma-poor histology over 50% (Luksch et al, 2016).
Furthermore, this class could be divided into three subtypes:

- Undifferentiated NB: undifferentiated neuroblast without recognizable neuropil
- Poorly differentiated NB: made up with cells with a recognizable neuropil
- Differentiated NB: identify with 5% or more tumour cells differentiated towards ganglion cells

The heterogeneity of neuroblastoma leads to wide clinical heterogeneity among patients, ranging from spontaneous regression of the tumour to a more aggressive form leading to a poor prognosis.
The most aggressive phenotype is characterized by the undifferentiated neuroblastoma type, as these high-risk cases are also the most frequent and often with the worst clinical outcome (Tonini et al, 2016).
The low-risk neuroblastoma is often associated with whole chromosomal abnormalities and, on the other hand, the high-risk cases show segmental chromosomal aberration that affect only some part of it.
The most remarkable neuroblastoma drivers are the activating of *ALK* mutations and *MCYN* amplification, which are the molecules driving the developing of neuroblastoma in animal models.

In addition to these, the overexpression of LIN28B is correlated with tumour development, mediating the downregulation of *Let-7* family of microRNAs resulting in overexpression of MycN protein.

1.1.7 MYCN amplification

The worst outcome in neuroblastoma is often associated with amplification of the *MYCN* gene (Maris et al, 2010). This gene encoding MycN protein is highly expressed in early stages of post migration of neural crest cells and plays a major role in cell proliferation and apoptosis during the normal sympatho-adrenal development. Thereafter, during the maturation of sympatho-adrenal precursor cells and their differentiation into neural or cromaffine cells, the level of MycN is gradually reduced.
Furthermore, it has been noted that during the final stages of sympatho-adrenal development there is an increase in progenitor cell proliferation that subsequently goes into controlled apoptosis.
Thus, it appears that MycN overexpression during these phases results in a blockage of apoptosis of sympatho-adrenal precursor cells, leading to their continued growth and eventually arising in neuroblastoma development (Johnsen et al, 2019).
Different studies were conducted in mice or zebrafish models, showing that the forced MycN overexpression in primary NCC led to the development of neuroblastoma. Hence, this result suggests that the amplification of MycN in NCC is sufficient for the neuroblastoma onset and makes it widely usable as biomarker for neuroblastoma risk categorization (Johnsen et al, 2019).
In human neuroblastoma it has been shown that there is a linkage between MYCN and its antisense RNA called MYCNOS (that encode N-CYM), indeed always be co-expressed and co-amplified, because N-CYM stabilizes the N-MYC inhibiting the degradation of the latter. The positive feedback between the MYCN/NCYM-amplified tumours, emphasises the aggressiveness of human neuroblastoma (Matthay et al, 2016).
Yosuke Sugenaga et al. (2014) have shown in their studies in MYCN transgenic mice a spontaneous generation of neuroblastoma with low appearance of metastasis compared to the human neuroblastoma condition. With a MYCN/NYCM double transgenic mice, it was found instead a metastasis presence, suggesting a crucial role of N-CYM in the development of tumours migration.

1.1.8 ALK mutations

Somatic mutation of Anaplastic Lymphoma Kinase (ALK) gene have been found in 14% of high risk-neuroblastoma. Mutation on *ALK* and *PHOX2B* are usually connected with familial neuroblastoma

presenting a hereditary form of neuroblastoma; the two mutation alleles are quite rare and are inherited in an autosomal dominant Mendelian way (Matthay et al, 2016).
ALK gene is a tyrosine-kinase receptor that also belongs to the insulin-receptor superfamily. When wrongly activated, it behaves like oncogene, altering mammalian cells both in vivo and in vitro (Luksch et al, 2016). The bond between *ALK* and *MYCN* might be due to the ALK mediation of cytokine kinase receptors signalling which leads to an increase of N-MYC levels (Matthay et al, 2016). Both *MYCN* and *ALK* are strongly expressed during human embryonic development and after birth their expression decreases over time, in fact they are not remarkable in adult tissues (Tonini et al, 2016).

1.1.9 Overexpression of LIN28B

The LIN28B RNA-binding protein is normally expressed during embryogenesis by undifferentiated tissues and embryonic stem cells, where it regulates pluripotency and cell proliferation capacity and, as development continues, reducing its effects in progressively differentiated tissues (Tsialikas et al, 2015). The role of this stemness regulator during embryogenesis contributes to the maintenance of undifferentiated neuroblasts in neuroblastoma (Johnsen et al, 2019).
One of the most recognised targets of LIN28B is *Let-7* miRNAs, a family of microRNA which has a role in tumour suppression. Hance, an incorrect LIN28B expression may lead to the development of several types of cancer, as highlighted in different studies in mice models (Molenar et al, 2012).
In neuroblastoma, the overexpression of LIN28B appears in high-risk group with a presence of spread metastasis and with an overall poor survival. As shown in Corallo et al, 2019 work, in a transgenic zebrafish model a consistent MYCN expression in the sympatho-adrenal precursor cells was observed due to LIN28B overexpression in the PSNS. The downregulation of let-7 miRNA increases the MYCN protein expression ending with the development of neuroblastoma, confirming that LIN28B is correlated to MYCN-amplified neuroblastoma in cell lines (Powers et al, 2019).
Furthermore, sustained expression of LIN28B leads to a significant increase in the integrins ITGA5 and ITGA6. The former was already known to be associated with metastasis in neuroblastoma; the latter, which was already known to induce metastasis in other adult tumour types, was finally associated with cell migration in neuroblastoma. This underlines the importance of integrin-mediated premetastatic behaviour of neuroblastoma cells with overexpressed LIN28B (Corallo et al, 2019).

1.2 Neuroblastoma Models

One of the major limits in drug development for pediatric and adult cancer is the inefficacy and inconsistency between *in vitro* and *in vivo* testing results, due to the lack of investigation of the components that characterize the tumour microenvironment (TME), that cause only 1 in 10 drugs being approved by FDA to enter clinical trials (Nolan et al, 2020). Indeed, the two-dimensional cell culture condition lacks the multicellular systems that are in direct contact with the extracellular matrix components (ECM) and does not consider the complexity of the dynamic architecture of the tumour microenvironment, leading the transition from two-dimensional (2D) to *in vivo* pharmacological testing really critical and most of the time not successful (Corallo et al, 2020). The existing knowledge of neuroblastoma biology is still insufficient at the tissue level. Due to this, a projection of patient's response to new drugs or agents, as they often target complex cellular elements or activate different signalling pathways, is limited.

The most adopted strategy for pre-clinical studies involve the use of 2D cell culture systems where neuroblastoma cells are grown as monolayer and hence are deprived from the three-dimensional (3D) architecture present in a tumour. Moreover, to advance the understanding in tumour biology, pathogenesis and drug response at different levels (tissue, organ, organism), experimental models with physiological relevance to humans are essentials (Nolan et al, 2020).

Among these, we can identify syngeneic, xenograft and humanized animal models. Even though on one hand these models can provide insights into specific questions about the progression of the disease, on the other hand they lack to reproduce the physiological condition of the neuroblastoma patients (Seitz et al, 2012).

Murine models, typically a necessary stage before progressing therapies to clinical trials, are frequently used due to their genetic homology to humans (~ 80%), ability to be genetically manipulated to mimic human diseases, and complex multicomponent environment (e.g stroma, immune cells) (Ornell et al, 2019). Among the murine models we can note the syngeneic murine C1300 NB, which has an intact murine system, it is highly reproducible and low-cost effect. Unfortunately, this model lacks to recreate the biology or genetic of alternations of human tumors as it also does not arise during embryogenesis like the human tumor (Seitz et al, 2012).

Transgenic murine models (TH-MYCN and LSL-MYCN) overcome some of these disadvantages as they respect the human tumor biology and histology, in addition to genetic expressions and tumor localisation. On the other side, they are much more expensive and labour intensive, in addition to having supra-physiological levels of MYCN expression (Althoff et al, 2017).

The most recent Xenograft murine models, in which neuroblastoma cell lines have been injected to form ectopic tumour masses, well mimic the genetic complexity of human tumours, but they lack any interaction with human stroma as they are established from genetically homogeneous cancer cell lines. Moreover, the tumour development progresses quickly and does not possess the feature of multistage cancer progression (Mak et al, 2014). The incorporation of human patient tumour pieces by injection into immunocompromised mice leads to the arise of patient-derived xenografts, which retain features of human neuroblastoma (i.e. histopathology, TME architecture and gene expressions) but are limited by the absence of an intact immune system, in addition to high costs, labour and skills.

Recently, the use of zebrafish as neuroblastoma disease model has grown due to its low cost, ease to handle, quick development and facility of high-throughput screening of drugs, in addition to its convenience for imaging and live-tracking of cells in vivo thanks to its optical transparency (Corallo et al, 2016). The limitations in the use of this animal model are mainly linked to its elementary organ systems and disparity of physiological temperature, compared to the human body.

Therefore, even though all these models can help gaining a better understanding of tumor biology and are definitely fundamental for screening anticancer compounds of several tumours, they have, each one in different ways, significant shortcomings (Nolan et al, 2020). These *in vivo* models can replicate the metastatic processes in a living system but the identification of the single steps is challenging. We also have to highlight that the use of animal models can lead to issues with feasibility and ethical concerns.

The need for an improved understanding of the progression and treatment of cancer has pushed for increased accuracy and physiological relevance of *in vitro* tumor models. In contrast, *in vitro* tissue models can provide means for better systematic, repetitive, and quantitative investigations, even though capturing limited aspects of the tumor microenvironment (Katt et al, 2016).

Hence, to fill up the void between the 2D and *in vivo* systems, several 3D *in vitro* models have been created adopting different bioengineering methodologies. This approach tries to minimize the limitation of traditional cell culture techniques applied in cancer research applications allowing cell growth in both static and dynamic conditions, giving more importance to TME, ECM and cell composition in disease progression. Cancer cells grown on a monolayer of a 2D surface lose several signalling pathways important in defining cell's response in terms of growth, metabolism and differentiation.

In a study conducted in human cancer cell line MCF-7 and its multidrug resistance variant MDR-MCF-7, cells were cultured using 3D spheroids and 2D monolayer methods. The results shown a lower proliferation in 3D culture for both cell lines compared to 2D culture. Moreover, after administration of anti-cancer drug doxorubicin, MCF-7 grown in 3D model had reduced sensitivity to the drug compared

to the cell line seeded in 2D. MDR-MCF-7 cultured in the 3D model showed no response to drug treatment in addition to an increased invasive potential and in case of solid tumor, cancer cells were hypoxic and centred due to limited blood and oxygen supply (Faute et al, 2002 & Fischbach et al, 2007). Therefore, we can say that in a 3D *in vitro* system, cells can support each other and behave in a way that is similar to the *in vivo* system, considering adhesion, motility, invasiveness and metastasis of tumour cells. Advances in tissue engineering, biomaterials, microfabrication and microfluidics have led to a rapid growth of 3D *in vitro* tumour models. These tools permit to investigate also the physical interactions between invasive cancer cells and their 3D microenvironments and the cellular response to physical factors such as ECM stiffness, flow and sheer stress (Asghar et al, 2015). In a study conducted by Casey et al (2012), it has been demonstrated that the most effective and better-known protein hydrogel for cancer cell response to 3D matrixes with different stiffness is collagen hydrogels. Moreover, it has been noted that the cell migration through the ECM can be altered by the stromal collagen deposition and crosslinking, due to the fact that it defines the stiffness of tumour microenvironment (Asghar et al, 2015). Shear stress is another important factor to be considered in a 3D microenvironment. Indeed, shear forces can potentially change the response and migration of invasive cancer cells entering the circulatory system. From the literature, fluid flow and shear stress on cancer cells changed the migratory response of cells by reducing their motility altering the level of matrix protein expression in the microenvironment (Qazi et al, 2001).
Among the bioengineered techniques used for 3D tumour models we can note spheroids, bio-printing, scaffold-based platforms, hydrogels and microfluidic systems.

1.2.1 Multicellular Tumour Spheroids (MCTSs) and Bio-printing

One of the most recognized and well-characterized 3D cell culture platforms to grow cancer cell lines under low adherent condition is the multicellular tumour spheroid (MCTSs) model. MCTSs obtained by aggregation of neuroblastoma cell lines can closely reflect the *in vivo* features of tumour cells, respecting the production of ECM, cell-cell interaction, gene interactions and cellular heterogeneity (Corallo et al, 2020). In a study conducted by Mitchell et al (2017), the migratory and invasive potentials in neuroblastoma cancer cells has been assessed by using neuroblastoma cell lines embedded in 3D collagen gels, highlighting a correspondence between altered cellular morphology and invasive capability in the surrounding environment. In the 3D model, compared to 2D cultures, cells have been involved in the Rac signalling pathway, highlighting the importance of these structures for studying the tumor biology and progression.

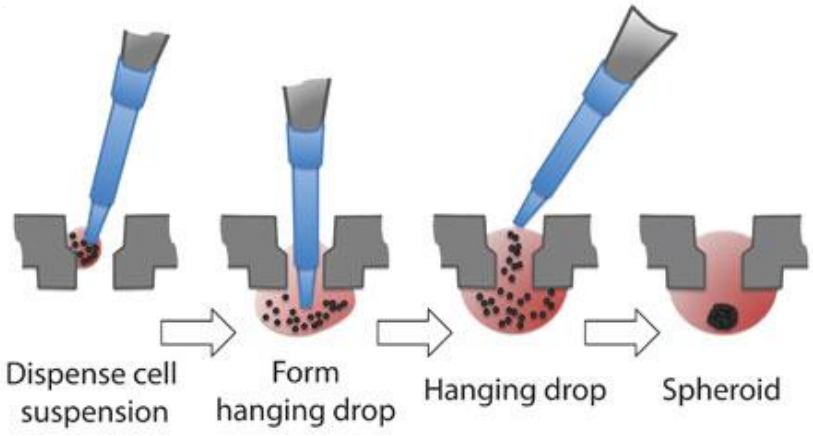

Fig 2: Hanging drop method to create a spheroid (Horman et al, 2013)

The production efficiency of spheroids, the influence of cellular physiology, the size uniformity and suitability for applications are the general criteria for selecting the spheroid method, even though the hanging drop is the most used to promote a natural aggregation (Asghar et al, 2012) (Fig.2). This method is inexpensive but challenging in terms of high throughput, droplet size control and uniformity and can lead to mechanical stress on cells. These platforms are suitable to investigate cell migrations and tumour invasive potentials, as well as the role of some proteins in the neuroblastoma resistance to anti-tumor drugs. On the other hand, MCTSs has some critical issues to consider, as the spheroid size and density affects the response to drug treatments (Nolan et al, 2020). Moreover, long-term *in vitro* culture of these cells is really challenging and in the end this model fails to truthfully mimic the complexity of neuroblastoma genetics (Corallo et al, 2020). Attempting to overcome the limitations of hanging drop methods, a more reproducible and efficient method has been used to lead the aggregation of spheroids, such as bio-printing technique. By using this approach, the control over spatial and temporal distribution of cell seeding is higher, even though, for successful results, inkjet and laser technologies have to meet certain design parameters to avoid damaging of pressure- and heat- sensitive biological fluids (Asghar et al, 2012).

The size of spheroids is important to replicate the tumor microenvironment. In a study conducted by Gransbury et al (2016), it has been assessed the different levels of hypoxia, diffusion and redox state of tumor cells within different microenvironments that were created in spheroids by changing the diameters, in a range from 50 to 800 μm. Moreover, it has been noted that spheroids are advantageous once they reached a critical size of > 100 μm, as they begin to show a microenvironment that changes due to nutrient and oxygen gradients.

1.2.2 Scaffold-based platforms and hydrogels

Thanks to a further knowledge in the bioengineering field gained over recent times, some biomimetic matrices were developed to replicate the ECM component structure affecting the tumour cells behavior. These scaffold-based platforms are available in different materials, such as synthetic, semisynthetic and natural. Using this approach to design in vitro models for neuroblastoma research, the system permits to have a huge adaptability while taking advantage of the increased biological complexity.
On the other hand, there is a high variability for biological scaffold and synthetic ones can lead to a questionable cell-polymer interaction (Jensen et al, 2020).
Scaffold provides a porous 3D structural matrix to support cell proliferation, migration and differentiation, and have recently become a focus in neuroblastoma research field to mimic the tumor microenvironment by exploring bacterial nanocellulose, calcium phosphate and collagen-based 3D scaffolds (Nolan et al, 2020). In a study conducted by Remuzzi et al (2020), a culture of rat mesenchymal stem cells was cultured on flat culture supports and in the "Nichoid", an innovative three-dimensional substrate micro-engineered to recapitulate the architecture of the physiological niche *in vitro*, showing that the 3D distribution of cell volume had effect on the MCS structure and their mechano-biological response, reflecting their *in vivo* behaviour.
Strictly correlated to the scaffold-based platforms are the hydrogels, networks of crosslinked hydrophilic polymers that can autonomous self-assembly in tissue-like structures and swell in water maintaining their three-dimensional structure. These materials, according to Ullah et al (2015) study, must fulfil some requirements to be applicable. They must provide cell alignment and attachment, maintain cellular metabolic activities as well as replicate cell response to mechanical and chemical stimuli in tissue. There are different biomaterials that can be used for this construct and the choice is related to the tumour type and other important physical parameters, for instance elasticity and stiffness. Among these materials we can count collagen, hyaluronic acid, alginate, agarose, gelatin, fibrinogen, PLGA, PEG, Pluronic F127, PLC, GelMa (Corallo et al, 2020). Hydrogels can be used to investigate cell migration as they mimic the ECM structure of the tumour and are characterized by tunable properties; recently they have been used to study neuroblastoma cell morphology and invasion (Nolan et al, 2020). Indeed, in the study by Yeung et al, the 3D neuroblastoma environment has been engineered by co-micro-encapsulation of tumor cells with mesenchymal stem cells (supportive stromal niche) in liquid collagen drops/microspheres (3D scaffold). This structure has led to neuroblastoma cell proliferation, irregular tumor outgrowth, tumor invasion and vascular spaces, representing the common

feature of *in vivo* tumor. On the other hand, hydrogel present as well some limitations, mainly linked to a lack of mechanical strength and a low reproducibility (Corallo et al, 2020).

1.2.3 Bioreactors and MOAB

To study the pathological environment of a disease, some engineered models have been proposed for investigating *in vitro* the tumour biology, immunology as well as the efficacy of new drug treatment, in order to gain a better understanding of the complexity of tumour progression (Corallo et al, 2020). By using miniaturized bioreactors, the culture *in vitro* of tumour cell lines can be achieved with a small number of cells and volume of reagents and be easily adapted with existing devices or platforms for High Throughput Drug Screening (Izzo et al, 2019). Indeed, in order to reproduce neuroblastoma vasculogenic mimicry, pre-vascularized neuroblastoma sheets seprated by fibrin layers has been used in perfusion bioreactor in order to recreate a complex *in* vitro model. In this study by Villasante et al (2017), cell sheets were fabricated by co-culturing the SK-N-BE neuroblastoma cell line with human umbilical vein endothelial cells (HUVEC) on temperature-responsive poly(N- isopropylacrylamide) (PIPAAm)-grafted culture plates and using collagen-gel base with microchannels as a support for the vascular bed. This structure allows to mimic the native tumor environment while increasing the predictivity for translation in pre-clinical applications. Even though this system has interesting outcomes, the difficulty of reproducing and stacking the cell-sheet and the hard labour required to assembly the collagen-base with microchannels for the perfusion set limits to the application of this model. As stated, a critical point in cancer progression is represented by the invasion of tumor cells into the surrounding tissue, and in some cases to metastasis in distant sites. In order to better understand and investigate the tumor invasion potential with higher-dimensionality descriptors than population-based assays, microfluidics systems can be relevant tools. In a study conducted by Lin et al (2017), the use of a microfluidic platform that integrates measurements of invasive motility and protein expression for single cells, was used to investigate human glioblastoma tumor-initiating cells (TICs). To make these dual measurements on the same cell, the platform comprises a planar polyacrylamide microfluidic device housing microtrenches that are enclosed to form microchannels using a polydimethylsiloxane (PDMS) lid.

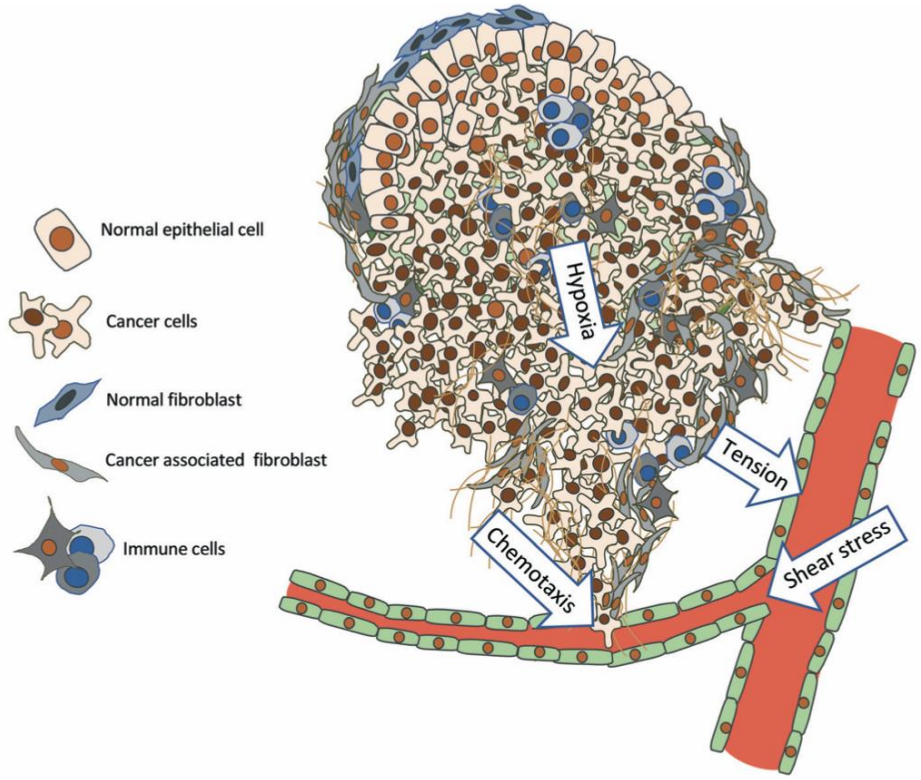

Fig.3: Schematic of a tumor system. Tumor progression is affected by microenvironment factors including mechanical and chemical such as shear stress, hypoxia, chemotaxis, cell–cell interactions, etc. These factors could be incorporated into tumor-on-a-chip models (Wan et al. 2019).

The major factors to take into consideration to recreate and examine a tumor-on-a-chip are the physiological relevant tumor-promoting mechanical forces: shear stress from the dynamic flow of vascular system, the tension from the solid tumor and stiffness of ECM. Moreover, the model can also provide insights about chemical factors, for instance chemotaxis due to nutrient diffusion and growth factor transduction as well as hypoxia gradient (Wan et al, 2019). (Fig.3)

Hence, Zou et al (2015) designed a V-shaped microfluidic device to track the migration of lung cancer stem cells and differentiated ones triggered by serum gradient. By using this system, they provide precise control of multiple gradient ranges as the cells showed consistent increase in migration distance. In a more recent study, Perottoni et al (2021) investigated the mesenchymal stem cell metabolism within a perivascular niche-on-a-chip, based on the coupling of a miniaturized in vitro system for human-MSCs dynamic culture such as MOAB (miniaturized optically accessible bioreactor) with high-resolution imaging of cell metabolism.

Indeed, one of the most recent devices that could investigate tumour complex etiology is the miniaturized optically accessible bioreactor, that permits to replicate both the 2D and 3D cell culture conditions in dynamic culture, leading to cell differentiation and reproducing *in vivo* behaviour (Izzo et al, 2019). Thanks to the optical transparency and low thickness of the components, it is optically accessible and may be exploited as a 4D bioreactor for prolonged culture. Moreover, it can be combined with analysis of the same constructs with time, by non-destructive techniques like fluorescence microscopy (Tunesi et al, 2019). These features make it suitable for the investigation of neuroblastoma cell lines, as it can study the behaviour of the tumor cells in response to different stimuli directly in a dynamic condition.

The limitations of using bioreactors as disease models can be linked to poor standardization, the need of specific read out and the fact that they cannot be always suitable for High Throughput Drug Screening (Corallo et al, 2020).

1.3 Aim of the study

The neuroblastoma origins are mostly known to be related to altered development of NCC.
The severity of the disease is intensely affected to its capacity of not only being related to primary tumour cells but instead of migrating into different body sectors (metastatic sites). The oncological research has been more and more focused on identifying the biological behaviour and cause of metastasis origins. In fact, recent studies pointed out an important correlation between the overexpression of LIN28B and the motility of neuroblastoma cells in zebrafish model (Corallo et al, 2019) and *in vitro* (Tao et al, 2020; Chen et al, 2020).
The aim of this study was to setup a miniaturized optically accessible bioreactor (MOAB) (Laganà et Raimondi, 2012) to allow real-time validation of the migratory and invasive phenotypes of human neuroblastoma SH-SY5Y cell line bearing ALK mutation and genetically modified to overexpress LIN28B (SH-SY5Y^{LIN28B}). Parental, genetically unmanipulated SH-SY5Y control cell line (SH-SY5Y^{CTRL}) expressing the gene at low level (Corallo et al, 2020).
The aim of the thesis was therefore to set up biological and engineering protocols that would permit the use of MOAB with nichoid scaffold-based structure as 3D *in vitro* model for investigating the molecular bases of the invasive phenotypes of neuroblastoma.
For achieve this goal, different biological and bioengineered factors were taken into consideration. Indeed, the major limits to overcome were:

- successful seeding of SH-SY5Y cell lines on MOAB chambers and 3D nichoid scaffold identifying the right number of cells to be cultured and amount of growth medium to be provided to their survival
- identifying the glucose consumption of SH-SY5Y tumor cells in both static and dynamic conditions inside MOAB chambers, respectively with an empirical and computational analysis
- estimating the correct flow rate of growth medium to be provided to MOAB chambers and the sheer stress that could be applied to cells, by using a computational method based on data achieved from previous studies
- choice of a suitable dye for fluorescence microscopy for living cell analysis

Therefore, after initial assessments for MOAB set up, we confirmed the viability of SH-SY5Y^{LIN28B} and control cell cultures in both 2D and 3D dynamic conditions, performing a LIVE/DEAD assay. Finally, we investigated the migration patterns of SH-SY5Y^{LIN28B} by performing an analysis of cells movement using time lapse imaging and qualitatively assessing their morphology compared to control neuroblastoma tumor cells through fluorescence microscopy.

2. Materials and methods

2.1 SH-SY5Y cell culture

Human neuroblastoma cancer cell line SH-SY5Y originally derived from a metastatic bone tumour biopsy (Biedler J.L. et al, 1973) were used in all the *in vitro* experiments. Morphologically, SH-SY5Y cell line in the undifferentiated form is characterized by neuroblast-like and non-polarized bodies, with few truncated processes. These cells are usually grown in clusters and may form clumps and cultures that contain both, adherent and floating cells (Kovalevich et Langford, 2013) (Fig.4).

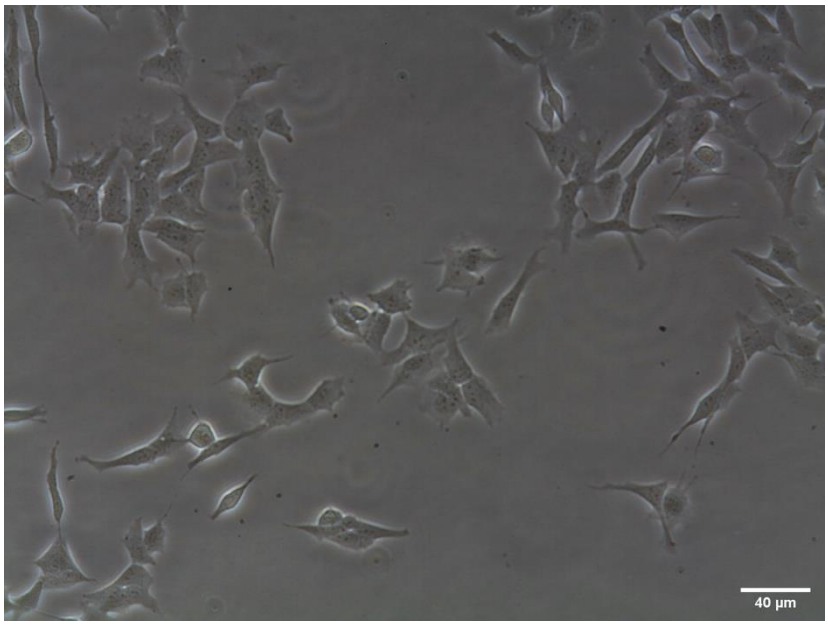

Fig. 4: SH-SY5Y cell morphology, 20X wild field microscope.

This neural crest-derived neuroblastoma cell line is characterized by a lack of expression of LIN28B in standard conditions, important feature for carrying out the experiments of this study, as recent works pointed out an important correlation between the overexpression of this gene and the motility of neuroblastoma cells in zebrafish neuroblastoma tumor model (Corallo et al, 2019) and in vitro (Tao et al, 2020; Chen et al, 2020).

In particular, SH-SY5Y were used as control cell line ($SH-SY5Y^{CTRL}$) against genetically engineered SH-SY5Y overexpressing human LIN28B under the control of a Doxycycline-responsive promoter ($SH-SY5Y^{LIN28B}$). More precisely, the overexpression was achieved upon the administration of Doxycycline at the concentration of 1 µg/mL for a period of 7 days.

Cell culture

Cells were cultured in RPMI (Sigma-Aldrich) medium in flask with the addition of 1% Glutamine (Gibco), 1% Penicillin/Streptomycin (Gibco) and 10% Fetal Bovine Serum (FBS; Gibco).
Cells were kept and maintained at 37°C with 5% CO_2 and 95% humidity.
The detachment of cells from the flask was carried out using the proteolytic enzyme Trypsin (Millipore), which hydrolyses peptide bonds between cells and ECM. The total cells number was identified by using an exclusion assay. An aliquot of 10 µL was picked up from the culture and the same amount of Trypan-Blue dye was added to the sample, in a proportion of 1:1 of cell mixture:dye. This method is based on the fact that Trypan Blue can only permeate and stain dead cells, making the recognition of living cells easier under a light microscope, as they appear bright and white.
The total amount of cells is then counted or automatically through the use of a cell-counter (CountessTM – Invitrogen), or manually by using a Neubauer cell.

In the manual method, the cells were counted in at least 4 squares of one of the two grids of the chamber. To determine the total number of cells available, was then applied the formula:

$$\text{Total Cell Number} = \frac{Counted\ CELLS}{Counted\ SQUARES} \cdot 2 \cdot TotalVOLUME \cdot 10^4$$

While to determine the cellular density (cell/mL):

$$\text{Cellular Density Counted} = \frac{Counted\ CELLS}{Counted\ SQUARES} \cdot 2 \cdot 10^4$$

2.2 Fluorescent Cell Labelling

Phalloidin Texas Red dye

Both the control cell line $SH-SY5Y^{CTRL}$ and the genetically modified cell line $SH-SY5Y^{LIN28B}$ for the overexpression of LIN28B under Doxycycline control, were put into chamber slides and fixed using 4% PFA in 1X PBS for 15 minutes. Then cells were washed one time with 1X PBS and permeabilized with 0,3% Triton X-100/ 1X PBS for 15 minutes. Samples were blocked with 5% BSA in 1X PBS for 30 minutes. Phalloidin Texas Red 1:200 in 5X BSA/ 1X PBS was added to the solution

and incubated overnight at 4 °C. At the end of the incubation, samples were washed three times with 1X PBS for 10' each. To counterstain nuclei, DAPI (1:1000, Invitrogen) was added to the solution for 10 minutes then washed again 3 times with 1X PBS. Finally, saellmples were mounted in 80% glycerol and analysed with ZEISS microscope and images processed with Fiji software.

Vybrant™ dye

Two different methods to labelling both cell lines $SH-SY5Y^{CTRL}$ and $SH-SY5Y^{LIN28B}$ with Vybrant™ were used to analyse the data in fluorescence assay.

Labelling of cells in suspension

After suspending cells at a density of $1x10^6$/ mL complete RPMI (Sigma Aldrich) medium with 1% Glutamine (Gibco), 1% Penicillin/Streptomycin (Gibco) and 10% Fetal Bovine Serum (FBS; Gibco), 5 µL/mL of Vybrant™ per mL of cell suspension was added with Hoechst diluted 1:1000 mL and incubated for 20 minutes at 37 °C. The cells were then centrifugated at 1500 rpm for 5 minutes and the supernatant removed and gently resuspended in the complete RPMI (Sigma Aldrich) growth medium, in a process repeated for 3 times.

Labelling of adherent cells

The complete RPMI (Sigma Aldrich) growth medium was removed from the culture cells and a staining medium was prepared by adding 5 µL/mL of Vybrant™ dye solution per mL of complete medium with Hoechst diluted 1:1000 mL. After adding the staining medium to the culture, the cells were incubated for 20 minutes at 37 °C. The staining medium was drained off, then new complete RPMI (Sigma Aldrich) growth medium was added and cells incubated for 10 minutes at 37°C.

Depending on the experiment conducted, after adding the dye, cells could be fixed by using 4% PFA for 15 minutes. Then cells were washed 3 times with 1X PBS for 10 minutes and samples mounted in 80% glycerol to be analysed with ZEISS microscope and images processed with Fiji software.

BacMam CellLight® proteins

The appropriate volume of BacMam CellLight® to be used to label both $SH-SY5Y^{CTRL}$ and $SH-SY5Y^{LIN28B}$ cell lines is calculated through the formula:

$$\text{Volume} = \textit{Number of cells} \cdot \frac{\textit{Desired PPC}}{1 \cdot 10^8\ \textit{CellLight® particles}}$$

where number of cells is the estimated total number of cells at the time of labelling, PPC is the number of particles per cell and $1 \cdot 10^8$ is the number of particles per mL of reagent.
After adding the right volume of BacMan CellLight® gently mixed, cells were incubated overnight. Depending on the experiment conducted, cells could be fixed by using 4% PFA for 15 minutes then washed 3 times with 1X PBS for 10 minutes. Finally, samples were mounted in 80% glycerol to be analysed with ZEISS microscope and images processed with Fiji software.

2.3 MOAB

The miniaturized optically accessible bioreactor (MOAB) (Fig.5) permits to replicate both the 2D and 3D growth of cell culture, enabling cell differentiation and reproducing *in vivo* behavior, while maintaining a continuous flow of medium and nutrient supply to cells (Izzo et al, 2019; Perottoni et al, 2021).

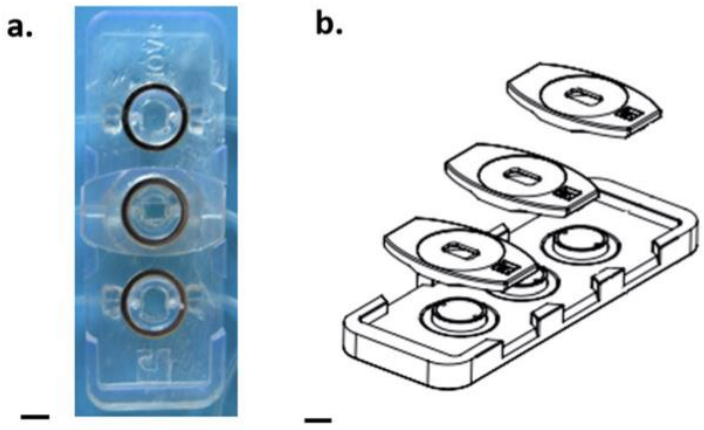

Fig. 5: Miniaturized optically accessible bioreactor (MOAB) (Izzo et al, 2019)
a. Top view of MOAB with magnetic closure
b. Technical sketch showing the MOAB with magnetic closure

The bioreactor was made of 3 independent chambers of 9 mm³ each with a glass coverslip attached to a silicone gasket, which shape permits to host differently shaped constructs. These chambers were

magnetically lockable and assembled on the top surface of a main medical grade polystyrene body of 68x25 mm. There were 2 different magnets that expose the cells to a static magnetic field, one NdFeB ring (12 mm outer diameter, 9 mm inner diameter, 1.5 thick) situated in the chamber and a second one located in the main body. The two magnets allowed the self-centering and self-aligning of the locking system, ensuring the hydraulic sealing during the perfusion of 3D constructs (Izzo et al, 2019).
The growth cell medium was pumped into the chambers with a flow rate of 1.0 × 10−3 mL/min and 5.0 × 10−3 mL/min by a multi-channel programmable syringe pump (SyringeSIX™, model NE-1600) in a gas permeable tubing system (Platinum-cured Silicone Tubing, 1/16 inner diameter, Masterflex) and collected in a reservoir after every single passage. The reservoir was linked as well to a 0.22 µm filter, able to maintain a zero pressure that guarantees a pressure gradient that permit the exit of fluids from MOAB. Depending on the experiments conducted, in the bioreactor chambers were applied structurally biomimetic 3D synthetic niches, or "nichoids", able to limit the dimension of the adhering embryoid bodies during expansion by counteracting cell migration between adjacent units of the substrate by its microarchitecture (Nava et al, 2016).
The structure of nichoid was characterized by blocks of 450 µm separated by corridors of 15 µm and divided in cells of 90 µm that were subdivided in small squares with a precise structure of 10, 20, 30, 20, 10 µm (Fig. 6).

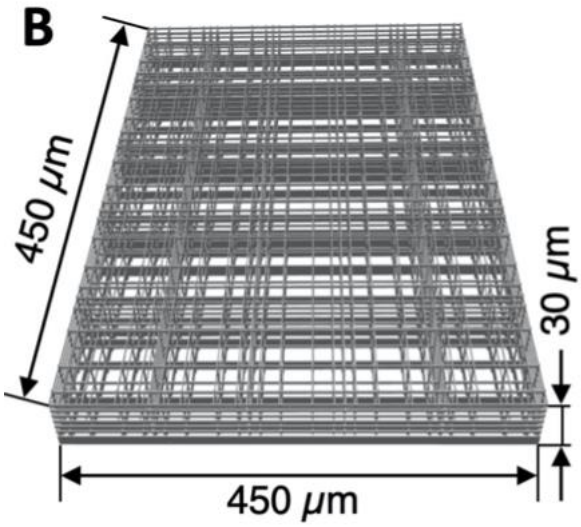

Fig. 6: CAD of one elementary block of the microfabricated 3D Nichoid structure (Remuzzi et al, 2020)

2.3.1 Modelling for dynamic culture

In order to compute the correct flow rate of complete growth medium to be pumped into MOAB chambers using the programmable syringe pump (SyringeSIX™, model NE-1600), we used a computational model made by COMSOL Multiphysics® software to individuate a potential critical sheer stress for plated cells that could affect their survival into the bioreactor.

The model simulates the structure of the MOAB culture chamber in its real dimensions in mm, with a central block attached to lateral arch shapes that correspond to the inlet tubes that permit the flow of the medium to the culture spot (Fig. 7).

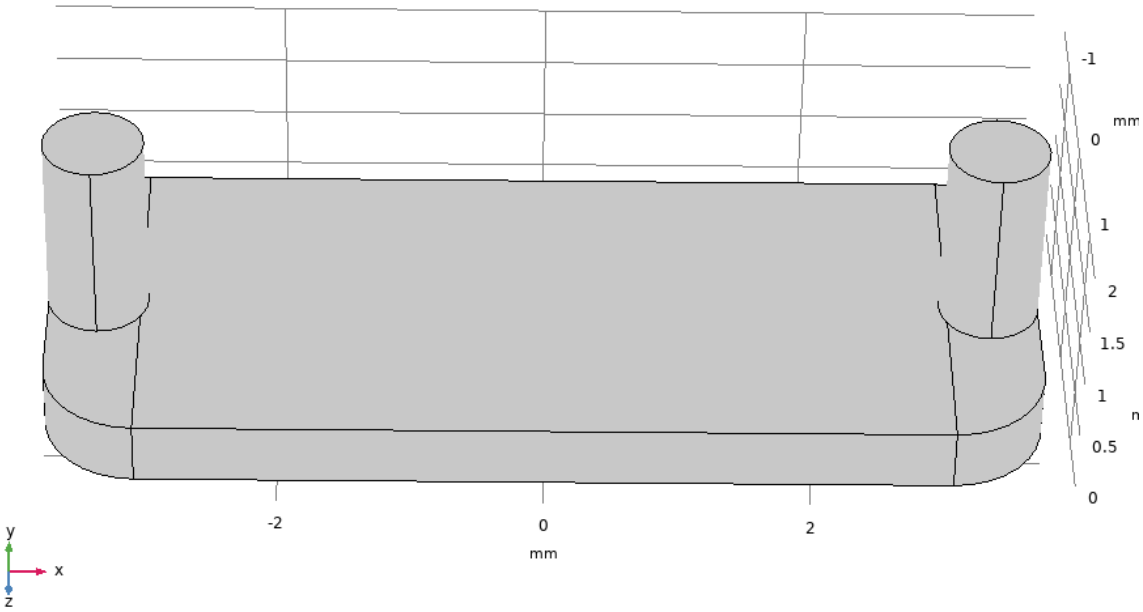

Fig. 7: CAD 3D of MOAB culture chamber model made by COMSOL Multiphysics®

A MOAB model created in SolidWorks was processed by COMSOL platform by using the parameters shown in Tab. 3.

Nome	Espressione	Valore
vin	0.00018 [m/s]	1.8E-4 m/s
d	1.5e7[1/m^2]	1.5E7 $1/m^2$
km	0.003 [mol/m^3]	0.003 mol/m^3
vmax	7.5e-17[mol/s]	7.5E-17 mol/s
D	5.4e-9[m^2/s]	5.4E-9 m^2/s
L	0.85e-3 [m]	8.5E-4 m

Tab. 3: Parameters used for COMSOL Multiphysics® MOAB simulation in dynamic conditions. vin = input speed, d = n° of cells in MOAB, km = Michaelis-Menten costant of Glucose, vmax = max uptake rate, D = diffusion coefficient of Glucose, L = inner diameter of tubes

This analysis mimics the dynamic of the continuous flow and the transport of diluted components in MOAB in order to identify the sheer stress applied to cells related to the flow rate chosen for the experiment.

The sheer stress [Pa] was calculated by using the formula:

$$\tau_{yx} = -\mu \frac{dv_x}{dy}$$

with μ = medium viscosity [Pa· s]; $\frac{dv_x}{dy}$ = velocity along x direction [m / s]

The Michaelis-Menten equation [mol/ h · cell] was considered to define the cell consumption of Glucose:

$$V = V_{max} \frac{c}{K_m + c}$$

with V_{max} = max uptake rate [mol/h · cell] ; c = concentration [mol/m^3]; K_m =.[mol/m^3]

2.3.2 MOAB set up protocol

After 7 days of treatment with Doxycycline, an aliquot of 50 000 cells was picked up from $SH-SY5Y^{LIN28B}$ cell line and suspended in 200 µL of RPMI growth medium (Sigma Aldrich) with 1% Glutamine (Gibco), 1% Penicillin/Streptomycin (Gibco) and 10% Fetal Bovine Serum (FBS; Gibco). The same process was applied to control cell line $SH-SY5Y^{CTRL}$.
Cell were therefore treated with the Vybrant™ labelling of cells in suspension protocol then plated directly in the MOAB chambers, one of which hosting the nichoid substrate, with the following scheme: 1st chamber $SH-SY5Y^{LIN28B}$, 2nd chamber with nichoid $SH-SY5Y^{LIN28B}$ and 3rd chamber $SH-SY5Y^{CTRL}$ as control. In this study the number of cells plated was in a range of 5000 to 20 000 cells. Before the transfer, the main body of the bioreactor was placed in two big different Petri dishes, to facilitate its transportation. Once treated with the dye, the cells were incubated at 37°C for 45 minutes, maintaining the correct humidity by placing stoppers full of water in the Petri dishes. At the end of this period, the complete growth RPMI medium was added to reach the full capacity of the chambers, up to 80 µL. Then cells were incubated overnight at 37°C.

The assembling of the MOAB was carried out starting from the outer components, linking the gas permeable tubing system (Platinum-cured Silicone Tubing, 1/16 inner diameter, Masterflex) to the reservoir and to the 0.22 µm filter for maintaining a stable zero pressure in the bioreactor chambers. The syringes mounted on a programmable syringe pump (SyringeSIX™, model NE-1600) were attached to the respective tubes and filled with 9 mL of RPMI growth medium (Sigma Aldrich) with 1% Glutamine (Gibco), 1% Penicillin/Streptomycin (Gibco) and 10% Fetal Bovine Serum (FBS; Gibco).
Eventual air bubbles were removed from the syringe by opening the clump and pumping medium out for all the tube length then tubes were clumped and attached to the MOAB main body.

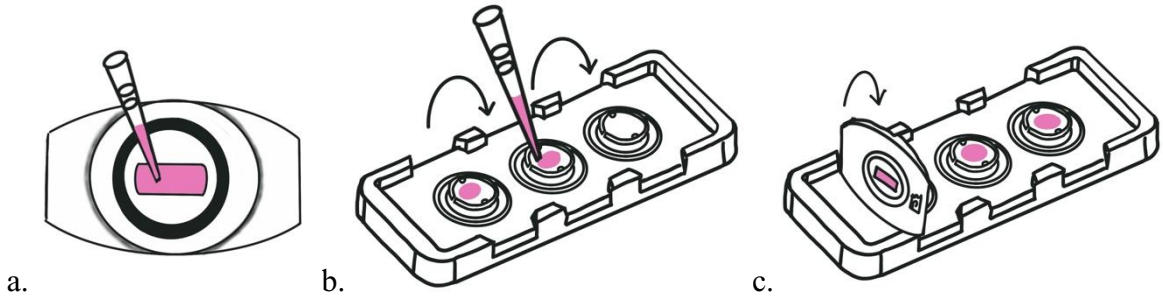

Fig. 8: Technical sketches of miniaturized optically accessible bioreactor (MOAB)

a. Top view of MOAB in the process of plating cells into one culture chamber **b.** Side sketch showing the main body of the bioreactor that in correspondence of the chambers is sprinkled with medium to avoid air bubbles formation during the chamber assembling **c.** Side sketch showing the assembling of MOAB chamber to the main body of the bioreactor

To also avoid the air bubbles formation during the assembling of the MOAB chambers on the main body of the bioreactor, complete growth medium was sprinkled in correspondence to the chamber's loci, as shown in Fig 8. The chambers with plated cells were then gently transferred into the predetermined loci of the bioreactor that was finally put in incubator together with the reservoir.
The syringes were attached to the pump that was set to a flow rate of 1.0×10^{-3} mL/min for 20 minutes then to 5.0 × 10−3 mL/min overnight, the clumps were removed, and the pump actioned (Fig. 9). After incubation, the chambers were analyzed with ZEISS microscope (Fig. 9) and images processed with Fiji software.

Fig. 9: MOAB assembled, during incubation (up). MOAB assembled, during observation (down).

2.4 LIVE/DEAD assay

The LIVE/DEAD is a viability/cytotoxicity assay based on the use of two probes that measure intracellular esterase activity and plasma membrane activity, determining the presence of live or dead cells in culture. The probes used to perform this assay were Calcein AM 4mM in anhydrous DMSO and Ethidium homodimer-1 (EthD), 2mM in DMSO/H_2O 1:4 v/v. After centrifugation, the probes were added to cells and incubated at 37°C for 45 minutes. Dead cells were labelled in red due to the binding of EthD to their DNA while living cells were stained with Calcein probe, as they generated a green fluorescence upon excitation of their cytoplasm. The data obtained were then analysed with a confocal FV10I microscope and images processed with Fiji software.

2.5 Time-Lapse

In order to follow cell migration over a period of time, a time-lapse analysis was performed. The quantification of displacement was measured in a 30 μm Z-Stack and tracked using Fiji software to determine the migratory and invasive phenotypes of SH-SY5Y^{LIN28B} cell line compared to the SH-SY5Y^{CTRL} cell line used as control. The MOAB chambers were analysed in 38°C heated chambers with ZEISS microscope and cell motility was captured over an 8h period at 30 minutes intervals while tracks were recorded using the Fiji "manual tracking" plug-in. The cell migration was determined by observing and measuring the formation of a straight-line distance from one cell first position to another point. Statistical analysis was conducted in Excel followed by a two-tailed Student's t-test; $p < 0.05$ was considered significant.

3. Results

3.1 MOAB set up

As we aimed to set up MOAB as 2D and 3D *in vitro* model in dynamic conditions for SH-SY5Y cell line, different factors were considered to identify the best conditions for the success of the experiment. The investigation was focused on the medium flow rate pumped into the MOAB chambers, the number of cells and medium culture to be used for seeding cells in the bioreactor, the choice of dye to visualise cells in fluorescence microscope.

3.1.1 Flow rate

Interstitial flow velocities in body tissues are generated from convective transvascular flows and are reported to range within 0.1–5 μm s^{-1} in physiological conditions, reaching up to 10 μm s^{-1} during inflammation, as stated in the studies of Perottoni et al (2021). In this work were analyzed different range of flow rates inside the MOAB for culturing MSCs in dynamic conditions, from 0.5 to 5 μm s^{-1}, to investigate the correspondent sheer stress inside the bioreactor. With a flow rate of 5 μm s^{-1}, the maximum value in physiological condition, the corresponding sheer stress detected was 0.001 dyne·cm^2, that was significatively lower than the values reported for sheer induced MSCs differentiation (Perottoni et al, 2021).

Therefore, according to the literature, in our study we chose an input flow rate of 5.0×10^{-3} mL/min, as it was the most convincing, considering the oxygen consumption across the culture chamber and we calculated the corresponding sheer stresses, obtaining the model shown in Fig.10.

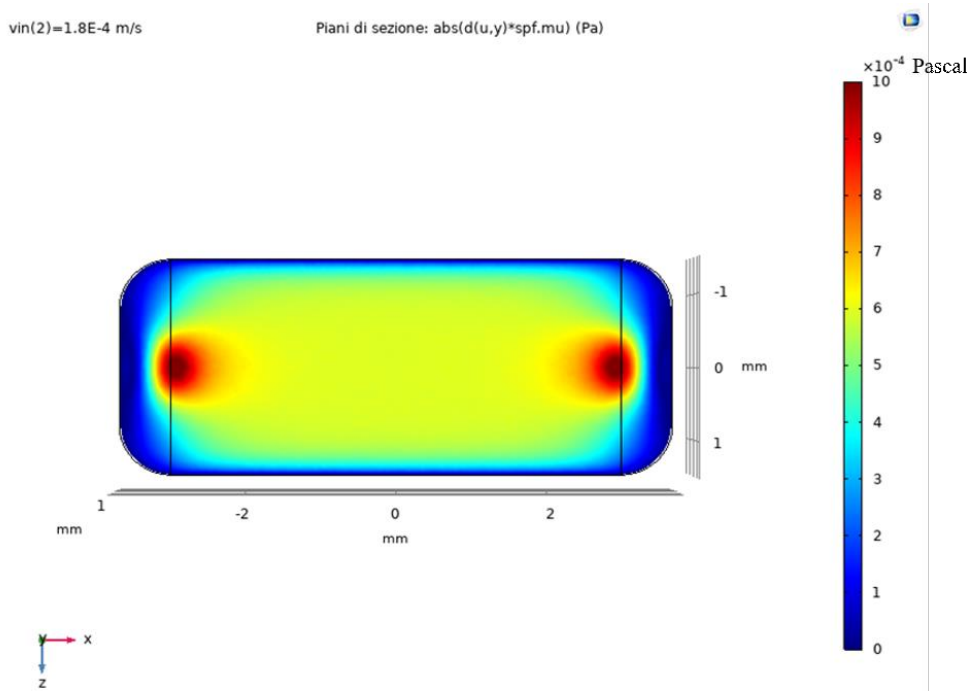

Fig. 10: Upper vision of MOAB culture chamber model made by COMSOL Multiphysics®. Operational condition with input flow rate (vi) of 5.0×10^{-3} mL/min. Scale bar representing sheer stress level in Pa.

By using an input flow rate of 5.0×10^{-3} mL/min, corresponding to the highest flow rate taken into consideration, the resulting sheer stress was 0,001 Pa. The velocity profile and the shear stress were uniformly distributed at the bottom of the culture chamber, predicting equal mechanical stimulation of shear stress to the cells.

Another factor to be considered for the cell's survival was the concentration of Glucose provided by the flow rate of complete growth medium into the MOAB chambers.
Using the Michaelis-Menten equation considering the Glucose consumption as output flow rate in the lower area of the MOAB chamber, we calculated the concentration gradient of Glucose inside the bioreactor and the obtained data was used in the computational simulation, as shown in Fig. 11.

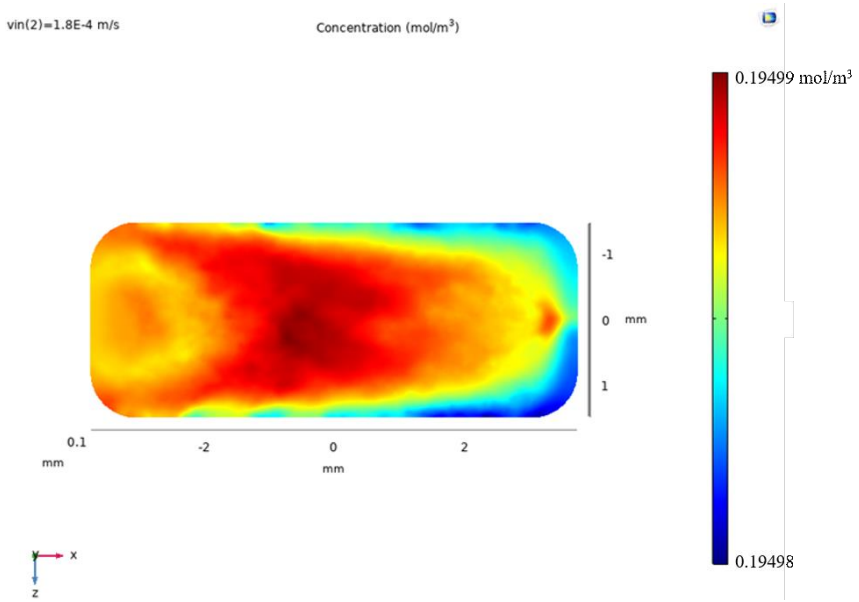

Fig. 11: Variation of glucose concentration in MOAB performed in a dynamic condition with 5.0×10^{-3} mL/min growth medium flow rate made by COMSOL Multiphysics®. Scale bar representing glucose concentration level in mol/m^3.

In simulations, the concentration of Glucose obtained was 0.19 mol/m^3.

As the maximum and lower values obtained were both approximate to 0.19 mol/m^3, we could be able to identify an equal distribution of Glucose concentration on the bottom surface of the MOAB chamber in stationary conditions with flow rate of 5.0×10^{-3} mL/min.

This value was way higher than the physiological need of Glucose corresponding to the consumption of this nutrient by cells seeded, as we know from literature that cells consume 0.05-2 µmol/h of Glucose every 10^6 cells in normal conditions for tumor cells.

3.1.2 Number of cells and amount of growth medium

To test whether the number of cells seeded into the bioreactor and the amount of complete growth medium added was ideal for cells' survival, we investigated different numbers of cells to be plated.

One of the crucial points for *in vitro* cell culture was to allow cell adhesion to a suitable substrate.

In order to pass from a static to dynamic culture of SH-SY5Y cell line in MOAB, we firstly attempted to find the best conditions for these neuroblastoma cell growth in a static environment then passed to a dynamic culture inside the bioreactor. Taking advantage of the triple structure of chambers present in the MOAB, in our experiments we added to one of them a scaffold-based construct, such as nichoid. This synthetic scaffold was used to simulate three-dimensional (3D) organization and migration of

neuroblastoma cells inside the bioreactor. The main variables of the experiments conducted for the MOAB set up were: number of cells of SH-SY5Y –both overexpressing LIN28B and control– seeded, the right amount of growth medium provided to cells and the presence of a coating to help the adhesion of the cells to the substrate. In the first experiments, in static conditions, we plated $15x10^3$ cells of both SH-SY5Y overexpressing LIN28B upon 7 days of doxycycline administration and control cells in glass slides with nichoid, to investigate the tumour cells morphology and behaviour in a 3D environment (Fig. 12).

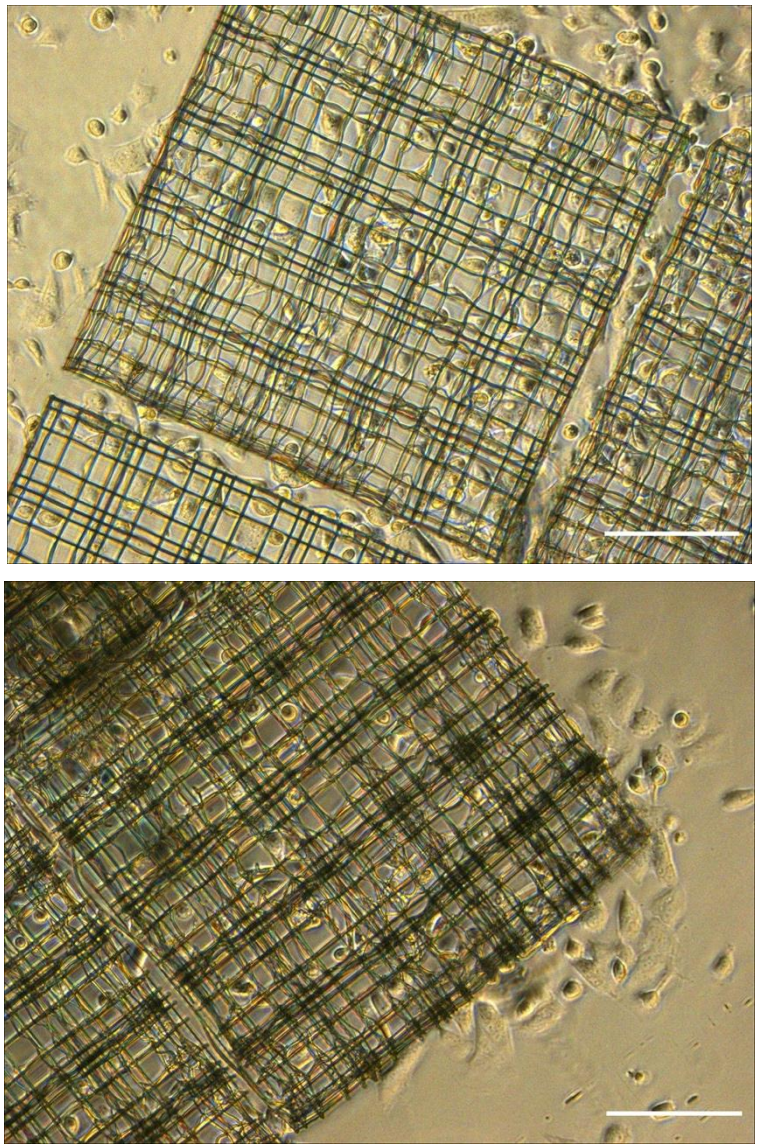

Fig. 12: Morphology of SH-SY5Y^{LIN28B} (up) cells treated with doxycycline for 7 days and SH-SY5Y^{CTRL} (down) control cells in nichoid. Bright-field images. Scale bar = 50 µm.

In order to have the best conditions to perform a migration assay, we decided to identify a proper range of cells seeded into the MOAB chambers, starting from a lower number compared to the one of the

glass slides. Therefore, we started seeding $2x10^3$, $3x10^3$ and $4x10^3$ SH-SY5Y^{CTRL} cells respectively in the three chambers of the bioreactor in 2D conditions and we analysed the samples with a bright-field microscope. Both after 5h incubation and overnight incubation, cells shown a rounded phenotype related to stress conditions and a not proper adhesion to the substrate. We thought that a possible reason for this condition could be linked to an insufficient number of cells seeded for having a proper cell density on the surface of MOAB chambers. Therefore, we passed to $5x10^3$ SH-SY5Y^{LIN28B} cells and SH-SY5Y^{CTRL} control cells into the culture chambers, and we added to the substrate a coating of Polyornithine and Fibronectin to enhance the possibility of cell adhesion to the glass. In fact, it is known from literature that these aminoacidic chains enhance cell attachment and adhesion to both plastic ware and glass surfaces (Dwane et al, 2013). Moreover, Fibronectin can just slightly affect the differentiation of SH-SY5Y cell lines, miming the environment of their substrate of adhesion (Dwane et al, 2013). Even in this case the adhesion of cells was not sufficient and the morphology was linked to a stress condition. Then the experiment was repeated by seeding a greater amount of both overexpressing and control SH-SY5Y cell lines, more precisely $10x10^3$ and $20x10^3$, but the results obtained shown the same issues as the previous ones (Fig. 13). At this point, we decided not to exceed the seeding of $20x10^3$ cells into the MOAB chambers in order to not affect the results of the migration assays with an excessive cell density in the bioreactor but we opted for take into consideration and investigate another parameter, such as the growth medium quantity.

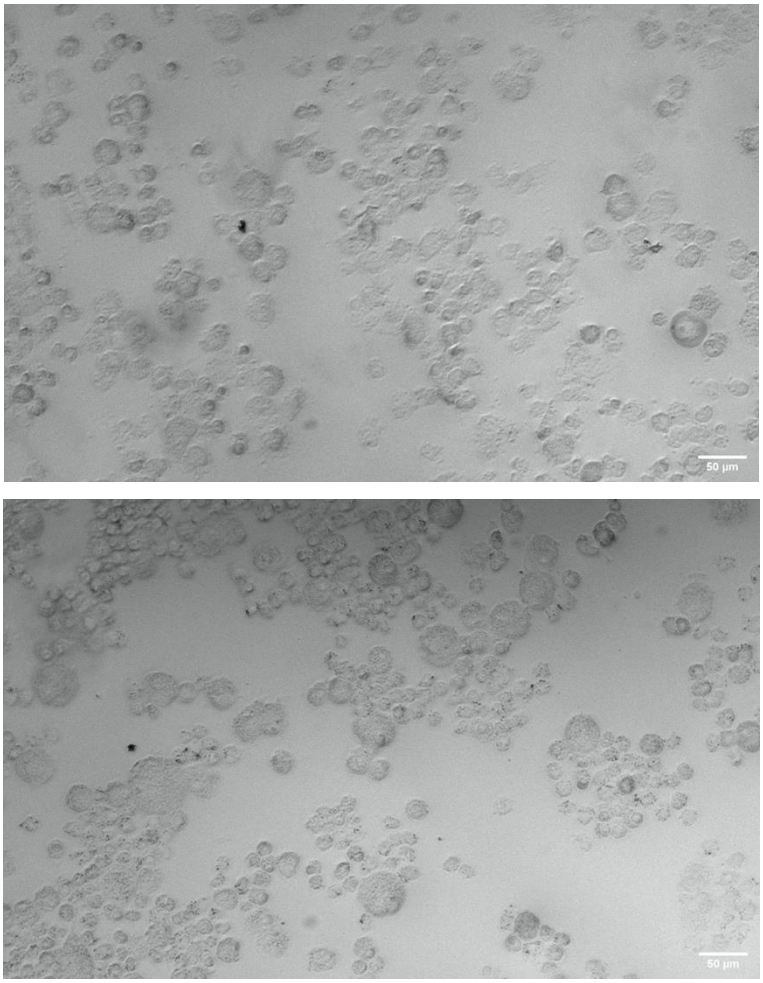

Fig. 13: Morphology linked to a stress condition of SH-SY5Y^{LIN28B} (up) cells treated with doxycycline for 7 days, and SH-SY5Y^{CTRL} (down) control cells. Arrows indicating the swelling and round shapes of cells. Bright-field images.

Finally, we passed testing the amount of growth medium provided to cells into the MOAB chambers to verify its influence on cells behaviour. As from our experiments both after 5h period and overnight incubation the cultures shown a poor or a lack of adhesion, we questioned if the amount of growth medium provided to cells was sufficient to permit their survival and attachment.

We decided to calculate the Glucose consumption of these cell lines in the MOAB chambers.

Considering that cells consume 0.05-2 µmol/h of Glucose every 10^6 cells and as we seeded 20 000 cells, the proportion was set as follows:

$$2\ \mu mol/h : 10^6\ cells = x : 20000$$

$$X = 0.04\ \mu mol/h\ required$$

As we usually used 40 µL of growth medium into the bioreactor, needed to cover the MOAB culture chambers, we determined that the amount of Glucose in this volume was of 0.2 µmol, therefore sufficient only for ~5h. From this statement, we increased the amount of complete RPMI (Sigma Aldrich) provided to the bioreactor until reaching the maximum culture chamber capacity, 80 µL.

We seeded again the SH-SY5Y cell lines, the one overexpressing LIN28B and the one for control, into the MOAB chambers considering this new variable and in an amount of $5x10^3$ and $10x10^3$ cells. We verified the conditions of cells after an overnight incubation with a bright-field microscope, assessing a good adherence to the MOAB chamber substrate and a phenotype relatable to traditional SH-SY5Y cell lines (Fig14).

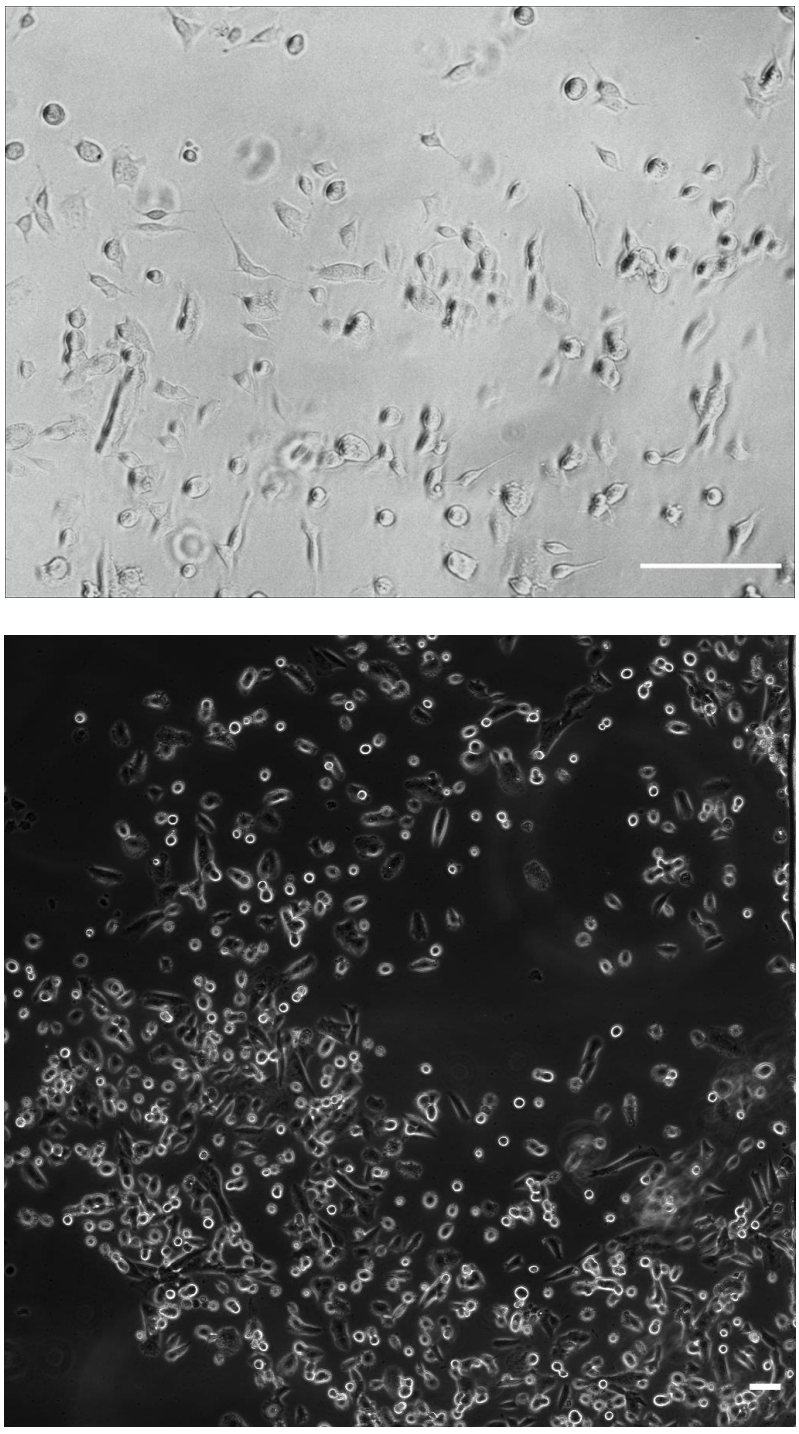

Fig. 14: Morphology of SH-SY5Y^{LIN28B} cells treated with doxycycline for 7 days right after seeding into MOAB chamber (up). Same chamber of MOAB showing SH-SY5Y^{LIN28B} cells morphology after an overnight perfusion (down). Bright-field images. Scale bar = 50 μm

3.1.3 Dye selection

Different dyes were tested to permit the visualization of cells and specific cytoskeletal proteins in order to identify cellular morphology and perform a migration assay in dynamic conditions through a fluorescence analysis. The dyes used were:

- Phalloidin: a selective bicyclic peptide used for staining actin filaments

- CellLight®: ready-to-use construct transfected into living cells for analysis

- Vybrant™: a dye delivery solution that can be added directly to normal culture media to uniformly label suspended or attached culture cells

From literature we know that long term LIN28B overexpression can lead to consistent morphology changes that are accompanied by a reorganization of cytoskeleton microfilament (Corallo et al 2019). Therefore, we decided to test which dye could best fit our dynamic conditions highlighting the cytoskeleton component of SH-SY5Y cell lines, trying to highlight their bigger and cuboidal shape compared to control (which were smaller and in stellated cell clumps), as described before (Corallo et al 2019). Phalloidin was used with SH-SY5Y culture in static conditions following a step of permeabilization of cell membrane and fixation of samples. This peptide conjugated with the fluorescent dye Texas Red® binds actin filament of the cytoskeleton and permits to visualize the morphology of the cells. The staining was performed for both SH-SY5Y cell lines, the one overexpressing LIN28B (in absence or presence of nichoid scaffold structure) and the one used as control (Fig. 15).

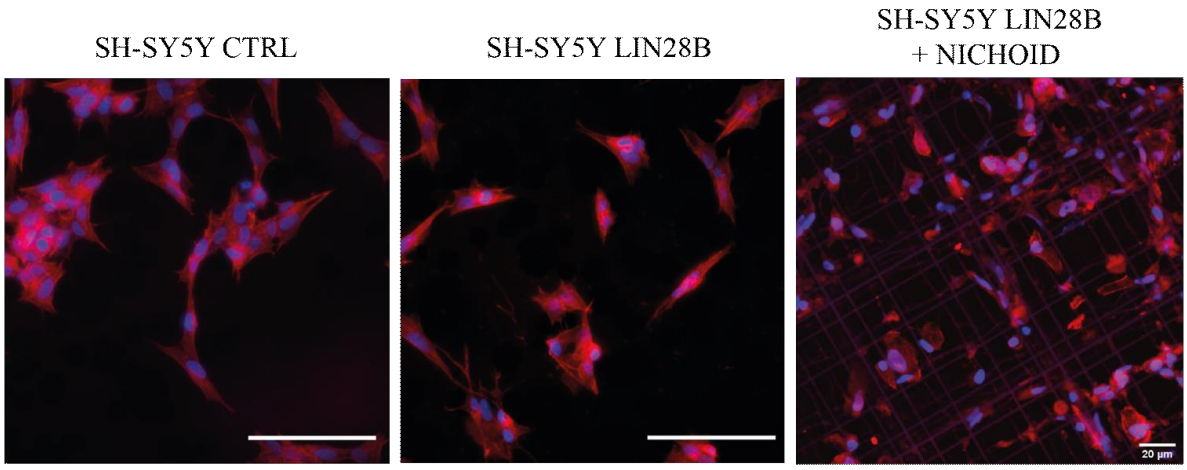

Fig. 15: Phalloidin staining of the SH-SY5Y^{CTRL} and SH-SY5Y^{LIN28B} upon 7 days of doxycycline administration in absence and presence of nichoid scaffold-structure. Scale bar = 50 µm. For SH-SY5Y^{LIN28B} with nichoid image scale bar = 20 µm.

SH-SY5Y^{LIN28B} cells showed a more geometrical and compact configuration compared to control cells, shape that was even more noticeable in neuroblastoma cells overexpressing LIN28B grown in nichoid. In order to perform a migration assay, the need of a dye suitable for the visualization of living cells was questioned. We considered both Vybrant™ and CellLight® dyes as good candidates for the labelling of SH-SY5Y cell cultures in dynamic conditions. Firstly, we conducted some experiments adding CellLight® following the standard protocol to the neuroblastoma tumour cell cultures in static conditions. This dye permitted to identify three different cytoskeletal proteins such as Actin (-GFP), Talin (-RFP) and Tubulin (-RFP) at cellular level, resulting to be a valid element for visualizing SH-SY5Y cell morphology (Fig. 16).

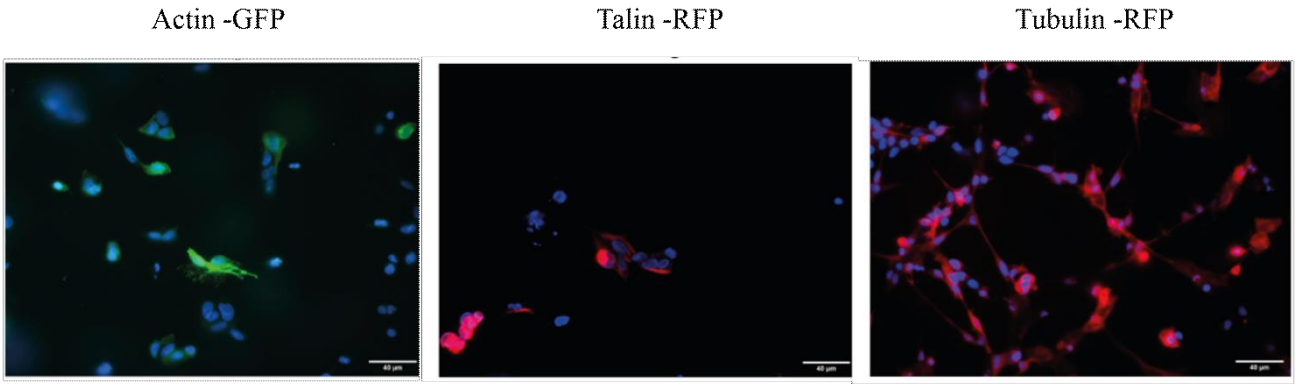

Fig. 16: CellLight® staining of SH-SY5Y^{CTRL} cell line with Actin, Talin, and Tubulin reagents.

On the other hand, to achieve the best results for the fluorescence analysis, we discovered that the quantity of PPC of dye to correctly perform the labelling was at the maximum value of its standard range of 10 to 50. Moreover, the best condition for having a right fluorescence was after 48h of incubation at 37°C. For these reasons, we decided to test Vybrant™ to find out a possibility of visualizing in a shorter time the SH-SY5Y cell cultures before passing to the assembling of the MOAB. This is due to the mechanical struggle of adding new dye after closure of the bioreactor but also to the difficulties noticed during the MOAB set up for maintaining a static long-term cell culture.

Therefore, Vybrant™ was added as well following its standard protocols to the static SH-SY5Y cell cultures and cells were visualized in fluorescent microscope, as shown in Fig. 17.

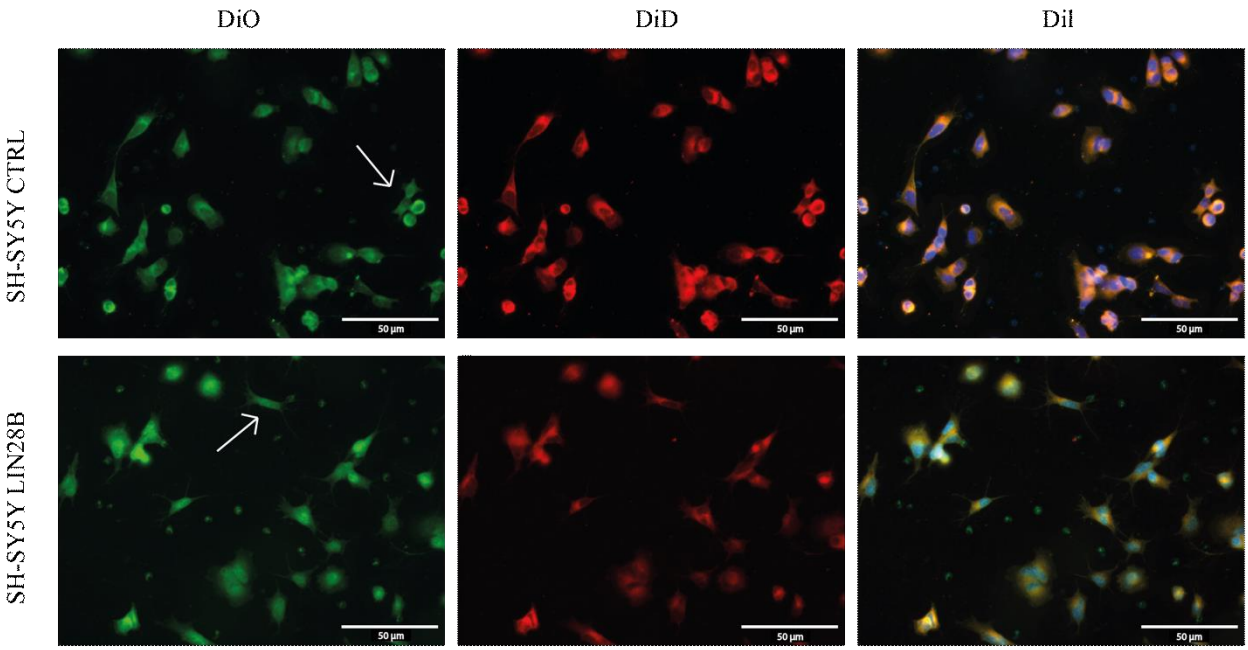

Fig. 17: Vybrant™ staining of the SH-SY5Y^{CTRL} and SH-SY5Y^{LIN28B} upon 7 days of doxycycline administration. Different reagents used: Dio (green), DiD (red), Dil (orange). Arrows indicating the different morphology of SH-SY5Y^{CTRL} (stellated-shape clumps) and SH-SY5Y^{LIN28B} (cuboidal shape).

We observed a difference in morphology between SH-SY5Y^{LIN28B} cells and control cells. The overexpressing LIN28B cells showed a rectangular parallelepiped shape compared to SH-SY5Y^{CTRL} that instead were seen in a grouped stellate-shaped configuration, confirming what stated in Corallo et al study (2019). Due to the technical issues observed with CellLight®, we decided to use the well-known Vybrant™ to conduct the other experiments of our study and to perform the analysis in dynamic conditions.

3.2 LIVE/DEAD assay

Once we determined the best conditions for SHSY5Y cell cultures in MOAB, we conducted the experiment following the protocol stated in the Material and Methods. Therefore, we performed a live dead analysis for identify the vital condition of cells in a dynamic environment with a continuous flow of 5.0×10^{-3} mL/min of growth medium injected by the pump syringe system.

Before carrying out this assay we stopped the flow rate and dissembled the bioreactor to permit the mechanical operations. The assessment was performed after 72h of dynamic condition and the images were processed with FV10I confocal microscope. By using Fiji software, we processed LIVE/DEAD images and we were able to perform a count of live and dead cells (Fig.18).

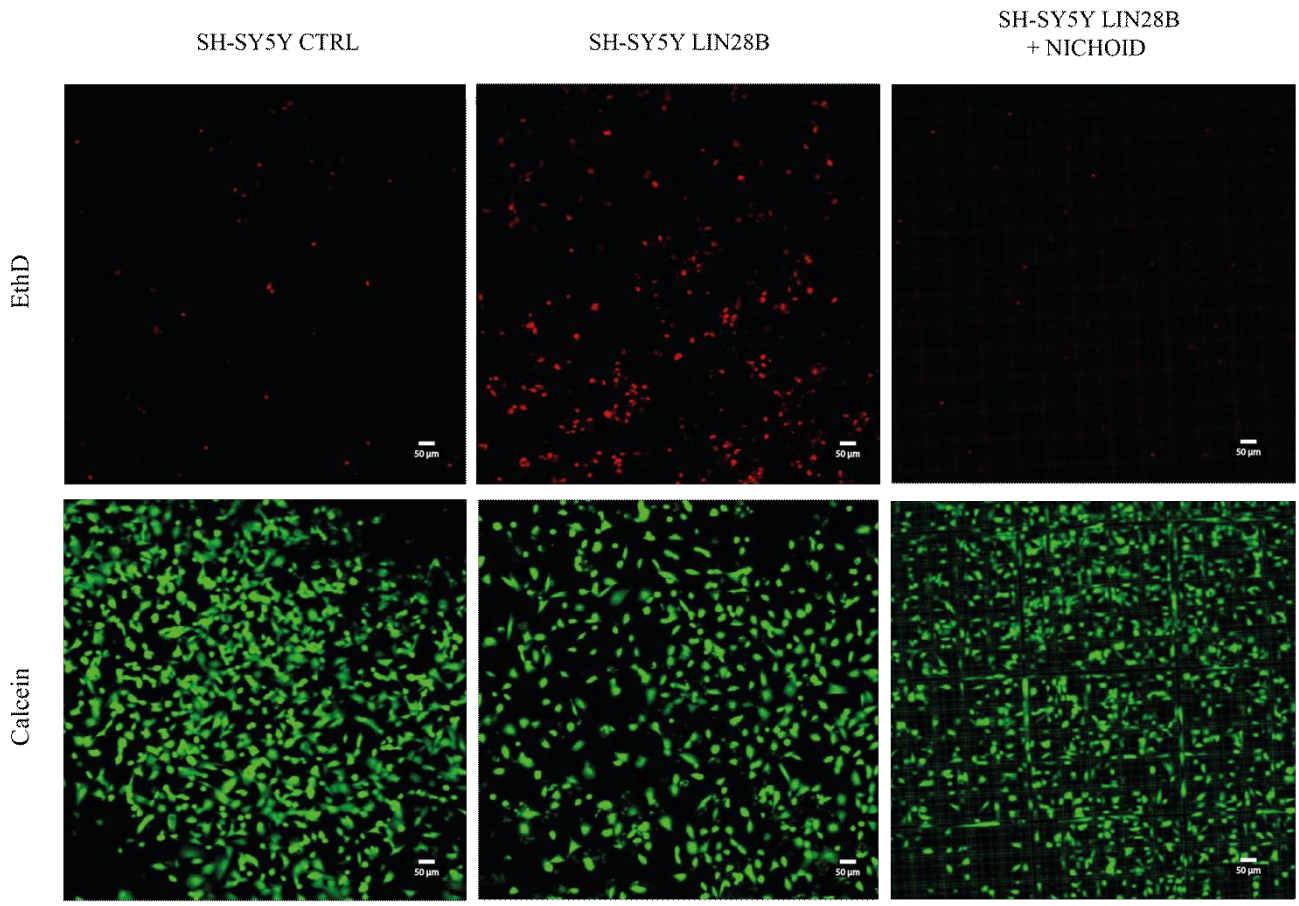

Fig. 18: LIVE/DEAD assay for SH-SY5Y^{CTRL} and SH-SY5Y^{LIN28B} upon 7 days of doxycycline administration in absence and presence of nichoid scaffold-structure. To each cell line correspond two images of a quadrant of the culture chamber with EthD staining dead cells in red, and Calcein labelling living cells in green.

Each MOAB chamber was divided into 9 quadrants for fluorescent imaging but for conducting the LIVE/DEAD analysis, we considered only the 3 images of the central part of the bioreactor chambers, as the later images were covering the outlines and the external parts of the MOAB chambers rather than only its internal surface.

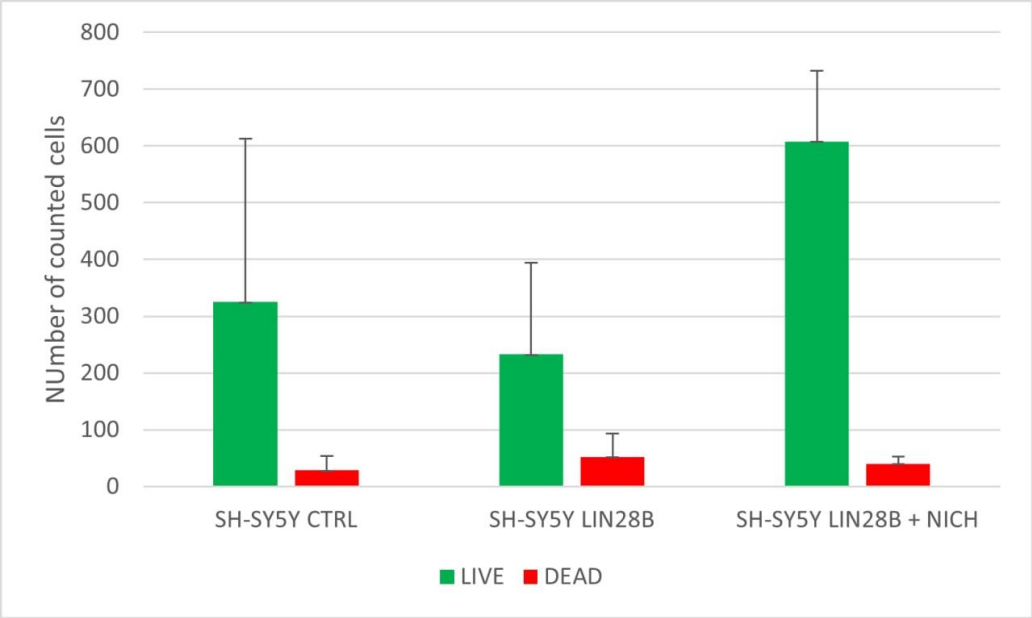

Fig. 19: Histogram of average number of cells counted in SH-SY5Y^{CTRL} and SH-SY5Y^{LIN28B} in absence/presence of a nichoid structure with LIVE/DEAD assay. The error bars represent SD.

The data obtained with Fiji software, as in Fig. 19, highlighted good results for both SH-SY5Y^{CTRL} and SH-SY5Y^{LIN28B} cell lines, with average numbers of cells counted of 325 ± 287 SD in SH-SY5Y^{CTRL}, 232 ± 161 SD in SH-SY5Y^{LIN28B} and 608 ± 124 SD in SH-SY5Y^{LIN28B} in nichoid.

The high values of SD were related to an uneven distribution of tumor cells in cultures, probably correlated to the difficulty of having uniformity and control during the seeding of cells by manual pipetting.

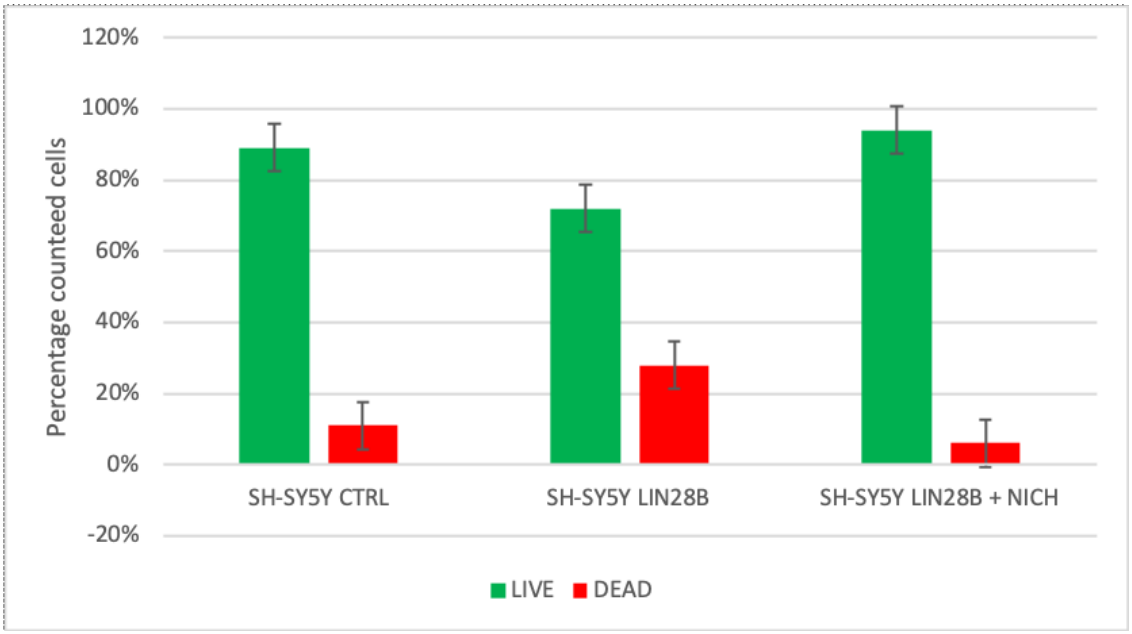

Fig. 20: Histogram of percentages of cells counted in SH-SY5Y^{CTRL} and SH-SY5Y^{LIN28B} in absence/presence of a nichoid structure with LIVE/DEAD assay. The error bars represent SEM.

In any case, we obtained high percentages of living cells corresponding to 92% for SH-SY5Y^{CTRL}, 82% for SH-SY5Y^{LIN28B} and 94% for SH-SY5Y^{LIN28B} in nichoid, as shown in Fig. 20. The slightly lower rate of vitality of SH-SY5Y cells overexpressing LIN28B was probably due to the presence of an air bubble inside the MOAB chamber that couldn't fade with the medium flow, therefore affecting the result of the assay. In any case, the vitality of cells was well confirmed after 3 days of flow perfusion indicating that the protocol chosen for the MOAB set up for SHSY5Y cells line permitted their survival and proliferation also in nichoid scaffold.

3.3 Time lapse and cells migration

From previous studies, we knew that the overexpression of LIN28B was established as a determinant factor for defining the migration of NNC cells, both *in vitro* and *in vivo,* also given the role of cytoskeleton reorganization in cell motility (Corallo et al, 2019).

Therefore, to assess a correlation between LIN28B overexpression and the increase of a migratory phenotype in neuroblastoma SH-SH5Y cell lines also *in vitro* dynamic conditions inside the MOAB, we performed an analysis of cells movement using time lapse imaging.

The overexpression of LIN28B in neuroblastoma SH-SH5Y was carried out over a long-term period of 7 days. The labelling obtained with the use of fluorescent dye permitted to analyse not only the morphology of SH-SY5Y^{LIN28B} and the corresponding controls (SH-SY5Y^{CTRL}), but also their movement in 2D and 3D (nichoid) dynamic conditions inside the bioreactor.

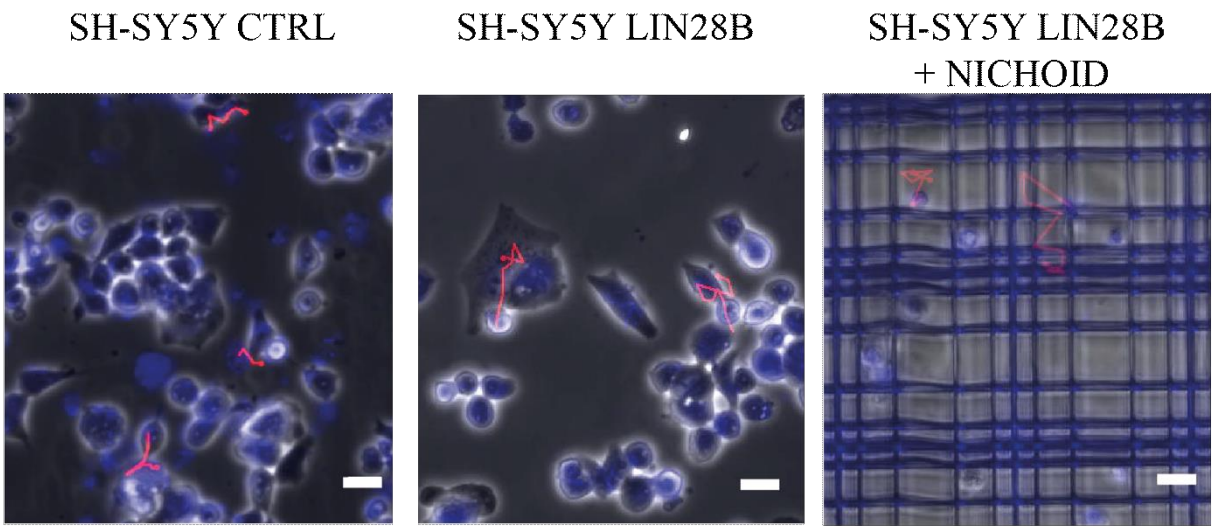

Fig. 21: Cell motility tracks of SH-SY5Y^{CTRL} and SH-SY5Y^{LIN28B} upon 7 days of doxycycline administration in absence and presence of nichoid scaffold-structure. Scale bar = 20 µm.

The results obtained shown an increase in migrated distances in SH-SY5Y^{LIN28B} cells compared to the control cell lines (Fig. 21). Considering the average distances, we could assess a significant difference between migration in µm between the SH-SY5Y^{LIN28B} and its control ($p=1.1x10^{-5}$), reinforced by the results obtained with SH-SY5Y^{LIN28B} seeded in nichoid ($p=1.8x10^{-5}$) (Fig. 22). By comparing the migration distances performed by SH-SY5Y overexpressing LIN28B seeded in a 2D and 3D (nichoid) culture in dynamic conditions inside the MOAB, we did not notice a significant difference (p=0.4).

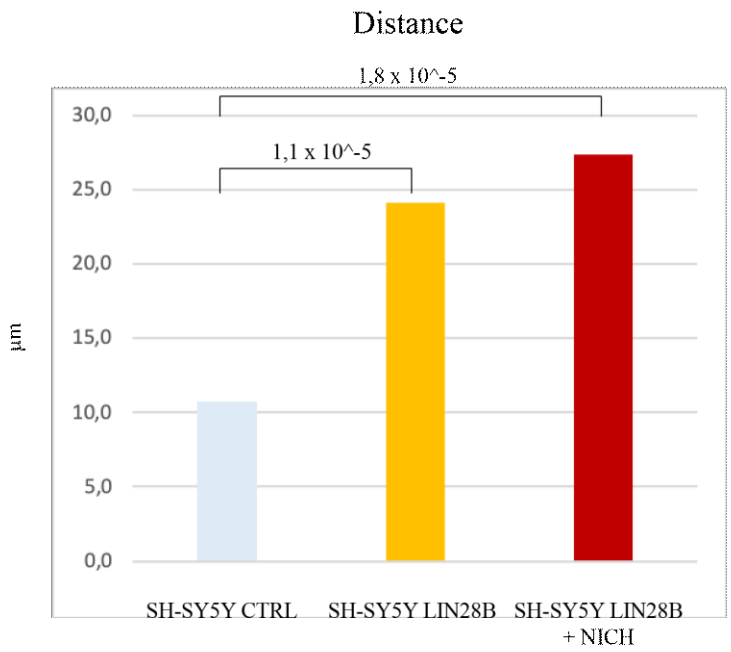

Fig. 22: Histogram of average migration distances (µm) of SH-SY5Y^{CTRL} and SH-SY5Y^{LIN28B} upon 7 days of doxycycline administration cells in absence/presence of a nichoid structure.
CTRL-LIN28B p = 1,1 x 10^{-5}. CTRL-LIN28B+Nichoid p = 1,8 x 10^{-5}

Moreover, it was registered an increase in the mean cell velocity of SH-SY5Y^{LIN28B} cells in a dynamic cell culture condition (Fig. 23).

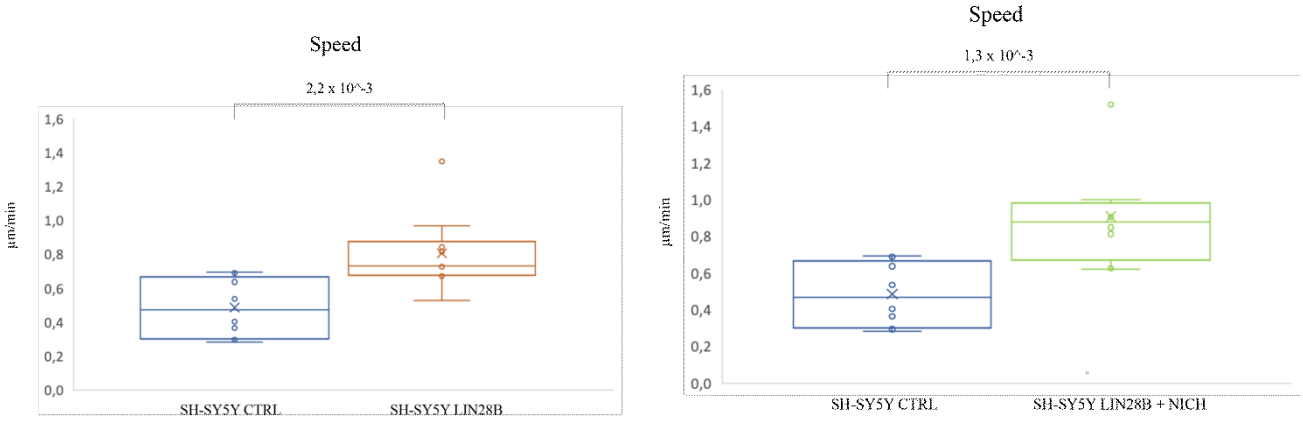

Fig. 23: a. Dot plots of average speed of SH-SY5Y^{CTRL} and SH-SY5Y^{LIN28B} upon 7 days of doxycycline administration cells, in µm/min. p = 2.2 x 10^{-3} **b.** Average speed (µm/min) of SH-SY5Y^{CTRL} and SH-SY5Y^{LIN28B} seeded in scaffold-based nichoid structure upon 7 days of doxycycline administration, depicted in dot plots. p = 1.3 x 10^{-3}

These increases reinforced the evidence stated from literature of the importance of LIN28B overexpression affecting the migratory capacity of SH-SY5Y, and were supported by statistical analysis ($p=2.2x10^{-3}$). The presence of a nichoid scaffold 3D structure for cells culture strengthened this evidence ($p=1.3x10^{-3}$). On the other hand, by confronting the speed of migration of SH-SY5Y^{LIN28B} cells both in absence and presence of nichoid construct in dynamic conditions, we did not notice a significant difference in migration ($p=0.4$).

4. Discussion

Neuroblastoma is a solid form of cancer developing from NCC system that represents 6-10% of all reported tumor cases in children under 5 years old, with an incidence of about 95% within this age (1:8000 live births) (Johnsen et al, 2019). About 40% of patients are diagnosed with neuroblastoma at 18 months and about 90% at less than 10 years of age. The age of diagnosis is strictly linked to prognosis, in fact patients with <18 months have much more probabilities of survival rather than other (Matthay et al, 2016), even though in many cases patients showing an initial good response to the used chemotherapy treatment suffer by relapse or drug- resistance (Luksch R. et al, 2016).
The biology and genetic of neuroblastoma are characterized by a high heterogeneity, influencing the clinical conditions of patients. The most aggressive phenotype is characterized by undifferentiated neuroblastoma cells, defining a category of high-risk cases that are mostly frequent and usually associated with the worst clinical outcome (Tonini et al, 2016). Indeed, these high-risk groups usually present metastasis, often involving lymph nodes, bone marrow and bone, and liver (Luksch R. et al, 2016). The most remarkable neuroblastoma drivers, according to animal models, are the activating of *ALK* mutations and *MCYN* overexpression. In addition to these, a key role has been attributed to *LIN28B,* an oncogene involved in the onset and progression of several types of cancer, as discovered in studies on mice models, characterized by high-risk groups overexpressing this RNA-binding protein (Molenaar et al, 2012). LIN28B regulates pluripotency and proliferation capacity and contributes to the maintenance of undifferentiated neuroblasts in neuroblastoma (Johnsen et al, 2019). Its pathological dysregulation in sympatho-adrenal precursor cells leads, as assed in zebrafish model, to an increase of neuroblastoma migratory capacity and promotes the invasive potential of the tumor (Corallo et al, 2019). Another important key role of neuroblastoma onset and malignancy is played by the extracellular matrix. The existing knowledge about neuroblastoma biology limits the projections on patient's response to new drugs, mainly because the 2D cell culture conditions lack the multicellular systems that are in contact with the ECM, not considering the complexity of the dynamic architecture of the tumour microenvironment (Corallo et al, 2020). New bioengineered methodologies have been applied to fill up this gap between 2D *in vitro* and *in vivo* systems, leading to 3D *in vitro* models as well as dynamic models. One of the most recent devices that could investigate the neuroblastoma biology, immunology and progression, is the miniaturized optically accessible bioreactor (MOAB) that due to its structure, permits to replicate *in vitro* both 2D and 3D culture in a dynamic condition, with a constant flow of growth medium provided to cells, miming this way *in vivo* behavior (Izzo et al, 2019).

The aim of this study was to setup MOAB to allow real-time validation of the migratory phenotypes of human neuroblastoma SH-SY5Y cell line overexpressing LIN28B (SH-SY5Y^{LIN28B}), compared to SH-SY5Y control cell line (SH-SY5Y^{CTRL}) expressing the gene at low level (Corallo et al, 2020). Toward this aim, after taking into considerations different variables (such us number of cells seeded, flow rate and amount of growth medium provided to cells, dye permitting the best evaluation of cells morphology), we were able to find a suitable protocol of set up for carrying out the migration assay of SH-SY5Y^{LIN28B} overexpressing LIN28B after 7 days of administration of doxycycline, compared to control. The evaluations done permitted to find the best conditions for the dynamic culture of SH-SY5Y cell lines in the bioreactor, in a future prospective of using this device as disease model.
By performing a migration assay of a 2D *in vitro* system in dynamic culture of neuroblastoma cell lines, we confirmed the increase of migratory and invasive phenotype of SH-SY5Y cells overexpressing LIN28B assessed by Corallo et al (2019). We observed indeed a significant difference between the average distance ($p=1.1 \times 10^{-5}$) and speed ($p=2.2 \times 10^{-3}$) of SH-SY5Y^{LIN28B} compared to the control. On the other hand, we were not able to identify a significant difference in terms of migration between the SH-SY5Y cell line culture in 2D and 3D (with nichoid) dynamic conditions.

We must underline that during the investigation, the migration of SH-SY5Y cells overexpressing LIN28B inside the nichoid was detected mainly inside the structures of the scaffold. The movement of cells indeed, was preferentially remaining within the structures of the scaffold rather than leaving their initial position, even though certain cells were able to go through nichoid grids. This finding confirmed the results of a study conducted by Remuzzi et al in 2020, where a culture of rat mesenchymal stem cells was cultured on flat culture supports and in the nichoid scaffold-base structure. After performing a migration analysis of MCS cells, the results pointed out that the flat control substrates allowed cells to migrate and explore the surroundings while cells on 2D nichoid showed similar speed and straight distance. On the other hand, cells on 3D nichoid showed lower distance travelled and lower straight distance as MSCs displayed a dynamic interaction with structural elements of the 3D nichoid grid, limiting the movement within the scaffold-based structure.
This is due to the fact that nichoid, with its 3D structure, as suggested by Remuzzi et al (2020), better mimics the complexity of tumour environment as it reflects also cell-cell and cell-ECM interactions (Nolan et al. 2020). Indeed, literature showed that 3D distribution of cell volume has a profound effect on mesenchymal stem cells structure and on their mechanobiological response, highlight the potential use of the 3D Nichoid substrate to strengthen the potential effects of MSC in vitro and in vivo

(Remuzzi et al, 2020). Therefore, in the future it could be interesting to compare the results obtained for SH-SY5Y^{LIN28B} in nichoid also with control cells culture in same 3D dynamic conditions, to better understand the pattern of migration of cells inside the scaffold.
The achievement of good condition for MOAB set up for SH-SY5Y cell lines could establish a new approach to overcome the limitations of the mostly and well-know 2D protocols for tumor research.
In fact, 3D culture and dynamic conditions could exploit the real advantages offered by neuroblastoma cell line models, giving more importance to TME, ECM and cell composition in disease progression.
Cancer cells grown on a 2D surface lose some signalling pathways that are important in defining cell's basal response in terms of growth, metabolism, and differentiation. Indeed, by using 3D structures the production of ECM, cell-cell interactions, gene interactions and cellular heterogeneity can be respected (Corallo et al, 2020). As one of the hallmarks of tumor progression and malignancy is represented by invasion of tumor cells into surrounding tissue, the use of 3D systems and microfluidics approaches can be relevant tools. From literature (Mitchell et al, 2017), the migratory and invasive potentials in neuroblastoma cancer cells have been investigated by using neuroblastoma cell lines embedded in 3D collagen gels, highlighting a correspondence between altered cellular morphology and invasive capability in the surrounding environment. By using the 3D model, compared to 2D cultures, it has been pointed the involvement of cells in Rac signalling pathway, highlighting the importance of these structures for studying and having a better understanding of the tumor biology and progression.

As stated, due to its capacity of increasing complexity and bio-mimicking cell-matrix interactions, the potential of 3D cultures could be even more exploited by a dynamic context simulating *in vivo* conditions, achieving a "4D dimension for long-term culture" (Tunesi et al, 2016).
The key factors of tumor-on-a-chip systems are the recreation of physiological relevant tumor-promoting mechanical forces: shear stress from the dynamic flow of vascular system, the tension from the solid tumor and stiffness of ECM. In addition to these features, the model can also provide insights about chemical factors, for instance chemotaxis due to nutrient diffusion and growth factor transduction as well as hypoxia gradient (Wan et al, 2019).
In this study we set a protocol to culture SH-SY5Y neuroblastoma tumour cell lines into a 2D and 3D dynamic condition, trying to recreate *in vitro* the *in vivo* condition of tumour biology and progression, overcoming the 2D and *in vivo* cultures limitations. The use of MOAB permits, due to its structure, to investigate at the same time both 2D and 3D cultures in a dynamic condition, leading to the achievement of different set of data corresponding to the independent chambers, for comparison.

By assessing a standard, repetitive and reproducible protocol, we aimed to ease further assessments with SH-SY5Y cell lines that could lead to interest results in terms of better knowledge of neuroblastoma cells behaviour, also in response to external stimuli.

The possibility of recreating a dynamic 3D neuroblastoma model could bring to a higher comprehension of the complex malignant tissue, deeply advancing the pre-clinical evaluation of new therapies for defeating tumour cells. By providing a protocol to be used as starting point, we tried to answer some questions regarding the possibility of screening the real key features that affects tumor development and how to integrate them into one simplified model (Wan et al, 2019). The possibility to conduct other studies with different neuroblastoma cell lines, could be interesting in order to understand the behaviour in a simil *in vivo* condition of different tumor drivers in addition to LIN28B overexpression. Indeed, from literature, we can note that also MYCN amplification (Maris et al, 2010) and ALK mutations (Matthay et al, 2016), are important contributors in neuroblastoma genesis, and have both been found in high-risk group patients. For this purpose, assessment with IMR32 cell lines with higher MYCN overexpression compared to other neurablastoma cells line such as SK-N-SH (Hiraiwa et al, 2019) could lead to interesting results, adding new and different variables to be integrated in this tumor-on-a-chip, therefore increasing the number of controllable parameters and variations of the system for improving treatment therapies.

Other interesting investigations could be done by studying neuroblastoma tumor cells behaviour in long-term culture, analysing their viability through LIVE/DEAD assays at different time period. Indeed, in this study the dynamic conditions were performed for maximum three days. There is therefore the need of conducting new studies with the same protocols to better understand its performance in a long-term perfusion. By achieving a long-term tumor cell culture in dynamic conditions we could confirm and extend the use of this protocol in MOAB not only for cell cultures but also for drug screening. Moreover, it could be interesting to investigate with this approach the recent "migrastatics" (Gandalovicová et al, 2017), a group of drugs that intervene in the invasion pathways of cancer cells leading to the subsequent formation of secondary tumours, by targeting essential mechanisms such as actin polymerisation and actomyosin contractility. For this reason, it will be necessary to continue investigating the potential of culturing cells in 3D inside MOAB for gain a deeper knowledge of the device and its application for neuroblastoma cell lines culture, aiming to improve tumour models, treatment therapies and disease testing methodologies.

5. Bibliography

1. Althoff K., Schramm A.; MYCN-mediated murine cancer models; Aging (Albany. NY) 9; 2017.
2. Asghar W., El Assal R., Shafiee H., Pitteri S., Paulmurugan R., Demirci U.; Engineering cancer microenvironments for in vitro 3-D tumor models; Materials Today
3. Biedler J. L., Helson L., and Spengler B. A.; Morphology and Growth; Tumorigenicity, and Cytogenetics of Human Neuroblastoma Cells in Continuous Culture; Cancer Res;1973.
4. Braekeveldt N., Bexell D.; Patient-derived xenografts as preclinical neuroblastoma models; Cell Tissue Res.; 2018.
5. Brodeur G. M., Pritchard J., Berthold F., Carlsen N. L.T., Castel V., Castleberry R. P., De Bernardi B., Evans A. E., Favrot M., Hedborg F., Kaneko M., Kemshead J., Lampert F., Lee R. E.J., Look A. T., Pearson A. D.J., Philip T., Roald B., Sawada T., Seeger R. C., Tsuchida Y., and Voute P. A.; Revisions of the International Criteria for Neuroblastoma Diagnosis, Staging, and Response to Treatment; American Society of Clinical Oncology; 1993.
6. Shawn P. Carey, Casey M. Kraning-Rush, Rebecca M.Williams, Cynthia A. Reinhart-King; Biophysical control of invasive tumor cell behavior by extracellular matrix microarchitecture; Biomaterials; 2012.
7. Chen D., Cox J., Annam J., Weingart M., Essien G., Rathi K.S., Rokita J.L., Khurana P., Cuya S.M., Bosse K.R., Pilgrim A., Li D., Shields C., Laur O., Maris J.M., Schnepp R.W.; LIN28B promotes neuroblastoma metastasis and regulates PDZ binding kinase; Neoplasia.; 2020.
8. Chu C. M., Rasalkar D., Hu J., Cheng W. T., Li K., and Chu W. C. W; Clinical presentations and imaging findings of neuroblastoma beyond abdominal mass and a review of imaging algorithm; The British Journal of Radiology; 2011.
9. Cohn S.L., Pearson A. D.J., London W. B., Monclair T., Ambros P. F., Brodeur G. M., Faldum A., Hero B., Iehara T., Machin D., Mosseri V., Simon T., Garaventa A., Castel V., and Matthay K. K.; The International Neuroblastoma Risk Group (INRG) Classification System: An INRG Task Force Report; Journal Of Clinical Oncology; 2009.
10. Corallo D., Candiani S., Ori M., Aveic S. and Tonini G.; The zebrafish as a model for studying neuroblastoma; Cancer Cell Int; 2016.
11. Corallo D., Donadon M., Pantile M., Sidarovich V., Cocchi S., Ori M., De Sarlo M., Candiani S., Frasson C., Distel M. Quattrone A., Zanon C., Basso G., Tonini G.P. and Aveic S.; LIN28B

increases neural crest cell migration and leads to transformation of trunk sympathoadrenal precursors; Cell death Diff; 2019.

12. Corallo D., Frabetti S., Candini O., Gregianin E., Dominici M., Fischer H., Aveci S.; Emerging Neuroblastoma 3D In Vitro Models for Pre-clinical Assessments; Frontiers in Immunology; 2020.
13. Delloye-Bourgeois C. and Castellani V.; Hijacking of Embryonic Programs by Neural Crest-Derived Neuroblastoma: From Physiological Migration to Metastatic Dissemination; Frontiers in Molecular Neuroscience; 2019.
14. Dwane S., Durack E. and Kiely P. A.; Optimising parameters for the differentiation of SH-SY5Y cells to study cell adhesion and cell migration; BioMed Central; 2013.
15. Faute M.A., Laurent L-, Ploton D., Poupon M., Jardillier J., Bobichon H.; Distinctive alterations of invasiveness, drug resistance and cell-cell organization in 3D-cultures of MCF-7, a human breast cancer cell line, and its multidrug resistant variant; Clin. Exp. Metastasis 19; 2002.
16. Fischbach C., Chen R., Matsumoto T., Schmelzle T., Brugge J., Polverini P., Mooney D.;Engineering tumors with 3D scaffolds;Nat. Methods 4; 2007.
17. French A. E., Grant R., Weitzman S., Ray J. G., Vermeulen M. J., Sung L., Greenberg M., and Koren G.; Folic acid food fortification is associated with a decline in neuroblastoma; Pharmacoepidemiology And Drug Utilization; Clinical Pharmacology & Therapeutics; 2003.
18. Gandalovicová A., Rosel D., Fernandes M., Veselý P., Heneberg P., Cermák V., Petruželka L., Kumar S., Sanz-Moreno V., Brábek J.; Migrastatics—Anti-metastatic and Anti-invasion Drugs: Promises and Challenges; Cell Press; 2017.
19. Gilbert & Barresi, Developmental Biology, Sinauer Associates, Inc., 2016.
20. Gransbury G.K., Kappen P., Glover C.J., Hughes J.N., Levina A., Lay P.A., Musgrave I.F., Harris H.H.; Comparison of KP1019 and NAMI-A in tumour-mimetic environments; Metallomics; 2016.
21. Hiraiwa T., Yamada T.G., Norihisa M., Funahashi A., Hiroi N.; Activation of cell migration via morphological changes in focal adhesions depends on shear stress in MYCN-amplified neuroblastoma cells; Interface; 2019.
22. Horman S.R., P.Orth A,, Slawny N., Cuddihy M., Caracino D.; 3D High-Content Analysis of Spheroids; Genetic Engineering & Biotechnology News; 15th Sep 2013.

23. Izzo L., Tunesi M. Boeri L., Laganà M., Giordano C., Raimondi M. T.; Influence of the static magnetic field on cell response in a miniaturized optically accessible bioreactor for 3D cell culture; Biomedical Microdevices; 2019.
24. Jensen C.; Teng Y.; Is it the time to start transition from 2D to 3D cell Culture?; Frontieres in Molecular Biosciences; 2020.
25. Johnsen J.I., Dyberg C. and Wickström M; Neuroblastoma—A Neural Crest Derived Embryonal Malignancy; Frontiers in Molecular Neuroscience; 2019.
26. Katt M.E., Placone A.L., Wong A.D., Xu Z.S., Searson P.C.; In Vitro Tumor Models: Advantages, Disadvantages, variables, and Selecting the Right Platform; Frontiers in bioengineering and biotechnology; 2016.
27. Kerosuo L., Bronner-Fraser M.; What is bad in cancer is good in theembryo: importance of EMT in neural crest development; Semin Cell DevBiol; 2012.
28. Kieuhoa T. V., Matthay K. K., Neuhaus J., London W. B., Hero B., Ambros P. F., Nakagawara A., Miniati D., Wheeler K., Pearson A. D.J., Cohn S. L., and DuBois S. G.; Clinical, Biologic, and Prognostic Differences on the Basis of Primary Tumor Site in Neuroblastoma: A Report From the International Neuroblastoma Risk Group Project; Journal Of Clinical Oncology; 2014.
29. Kovalevich J., Langford D.; Considerations for the Use of SH-SY5Y Neuroblastoma Cells in Neurobiology; Methods Mol Biol; 2013.
30. Lacayo N. J.; Coppes M. J.; Pediatric Neuroblastoma; Medscape; 2017.
31. Laganà M.; Raimondi M. T.; A miniaturized, optically accessible bioreactor for systematic 3D tissue engineering research; Biomed Microdevices; 2012.
32. J. M. G. Lin, C. Kang, Y. Zhou, H. Huang, A. E. Herr and S. Kumar; Linking invasive motility to protein expression in single tumor cells; Lab Chip; 2017.
33. Luksch R., Castellani M.R., Collini P., De Bernardi B., Conte M., GambiniC., Gandola L., Garaventam A., Biasoni D., Podda M., Sementa A.R., Gatta G., Tonini G., Neuroblastoma (peropheral neuroblastic tumours), Critical Reviews in Oncology/hematology; 2016.
34. Mahapatra S., Challagundla K. B.; Neuroblastoma; StatPearls Publishing LLC.; 2020.
35. Mak I.W.Y., Evaniew N., Ghert M.; Lost in translation: animal models and clinical trials in cancer treatment; Am. J. Transl. Res. 6; 2014.
36. Maris J. M.; Recent Advances in Neuroblastoma; The new England journal of medicine; 2016.
37. Matthay K. K., Maris J. M., Schleiermacher G., Nakagawara A., Mackall C. L., Diller L. and Weiss W. A.; Neuroblastoma; Nature Reviews; 2016.

38. Mitchell C.B., O'Neill G.M.; Rac GTPase regulation of 3D invasion in neuroblastomas lacking MYCN amplification; Cell Adh Migr; 2017.
39. Nava M.M., Piuma A., Figliuzzi M., Cattaneo I., Bonandrini B., Zandrini T., Cerullo G., Osellame R., Remuzzi A. & Raimondi M. T.; Two-photon polymerized "nichoid" substrates maintain function of pluripotent stem cells when expanded under feeder-free conditions; Stem Cell Research & Therapy volume; 2016.
40. Nolan J.C., Frawleya T., Tighea J., Soha H., Curtind C., Piskareva O.; Preclinical models for neuroblastoma: Advances and challenges; Cancer Letters; 2020.
41. Ornell K.J., Coburn J.M.; Developing preclinical models of neuroblastoma: driving therapeutic testing; BMC Biomedical Engineering; 2019.
42. Perottoni S., Neto. G.B., Di Nitto C., Dmitriev R.I., Raimondi M.T., Monaghan M.G.; Intracellular label-free detection of mesenchymal stem cell metabolism within a perivascular niche- on-a-chip; Lab on a chip, Royal Society of Chemistry, 2021.
43. Powers J. T., Tsanov K. M., Pearson D. S., Roles F., Spina C. S., Ebright R., Seligson M., de Soysa Y., Cahan P., Theißen J., Tu H., Han A., Kurek K. C., LaPier G. S., Osborne J. K., Ross S. J., Cesana M., Collins J. J., Berthold F. and Daley G. Q.; Multiple mechanisms disrupt the let-7 microRNA family in neuroblastoma; Macmillan Publishers Limited; 2016.
44. Raghu K. and Weinberg R. A.; The basics of epithelial-mesenchymal transition; The Journal of Clinical Investigation; 2009.
45. Remuzzi A, Bonandrini B., Tironi M., Longaretti L., Figliuzzi M., Conti S., Zandrini T., Osellame R., Cerullo G. and Raimondi M. T.; Effect of the 3D Artificial Nichoid on the Morphology and Mechanobiological Response of Mesenchymal Stem Cells Cultured In Vitro; Cells; 2020.
46. Seitz G., Armeanu-Ebinger S., Warmann S., Fuchs J.; Animal models of extracranial pediatric solid tumors; Oncol. Lett. 4; 2012.
47. Tao T., Shi H., Mariani L., Abraham B.J., Durbin A.D., Zimmerman M.W., Powers J.T., Missios P., Ross K.N., Perez-Atayde A.R., Bulyk M.L., Young R.A., Daley G.Q., Look A.T.; LIN28B regulates transcription and potentiates MYCN-induced neuroblastoma through binding to ZNF143 at target gene promotors; Proc. Natl. Acad. Sci.;2020.
48. Tonini G. P.; The Origin of Neuroblastoma; InTech; 2017.
49. Tsialikas J. and Romer-Seibert J.; LIN28: roles and regulation in development and beyond; The Company of Biologists; 2015.

50. Tunesi M., Fusco F., Fiordaliso F., Corbelli A., Biella G. and Raimondi M. T.; Optimization of a 3D Dynamic Culturing System for In Vitro Modeling of Frontotemporal Neurodegeneration-Relevant Pathologic Features; Frontiers in Aging Neuroscience; 2016.
51. Qazi H., Zhong-Dong S.,Tarbell J.; Fluid Shear Stress Regulates the Invasive Potential of Glioma Cells via Modulation of Migratory Activity and Matrix Metalloproteinase Expression; 2001.
52. Ullah F., Othman M.B.H., Javed F., Ahmad Z., Akil H.M.; Classification, processing and application of hydrogels: A review; Mater Sci Eng C; 2015.
53. Villasante A., Sakaguchi K., Kim J., Cheung N.K., Nakayama M., Parsa H., et al.; Vascularized Tissue-Engineered Model for Studying Drug Resistance in Neuroblastoma; Theranostics; 2017.
54. Wan L., Neumann C.A., LeDuc P.R.; Tumor-on-a-chip for integrating a 3D tumor microenvironment: chemical and mechanical factors; Lab on a chip, Royal Society of Chemistry, 2021.
55. Yeung F., Ho Yu Chung P., Kwong H.T.P., Kak Yuen Wong K.; Is complete resection of high-risk stage IV neuroblastoma associated with better survival?; J. Pediatric Surgery; 2015
56. Yusuke S., Islam S. M. R., Alagu J., Kaneko Y., Kato M., Tanaka Y., Kawana H., Hossain S., Matsumoto D., Yamamoto M., Shoji W., Itami M., Shibata T., Nakamura Y., Ohira M., Haraguchi S., Takatori A., Nakagawara A.; NCYM, a Cis-Antisense Gene of MYCN, encodes a De Novo Evolved Protein That Inhibits GSK3b Resulting in the Stabilization of MYCN in Human Neuroblastomas; PLOS Genetics; 2014.
57. H. Zou, W. Yue, W.-K. Yu, D. Liu, C.-C. Fong, J. Zhao and M. Yang; Microfluidic Platform for Studying Chemotaxis of Adhesive Cells Revealed a Gradient-Dependent Migration and Acceleration of Cancer Stem Cells; Anal. Chem.; 2015.